Biogeosciences Discuss., doi:10.5194/bg-2017-1, 2017
Manuscript under review for journal Biogeosciences
Published: 19 January 2017

Biogeosciences Discussions Open Access EGU

Spatial variability of surface-water pCO_2 and gas exchange in the world's largest semi-enclosed estuarine system: St. Lawrence Estuary (Canada)

Ashley Dinauer[1] and Alfonso Mucci

GEOTOP and Department of Earth and Planetary Sciences, McGill University, 3450 University Street, Montreal, QC H3A 0E8, Canada

[1] Corresponding author (ashley.dinauer@mail.mcgill.ca)

Abstract

The incomplete spatial coverage of partial pressure of CO_2 (pCO_2) measurements across estuary types represents a significant knowledge gap in current regional- and global-scale estimates of estuarine CO_2 emissions. The Estuary and Gulf of St. Lawrence (EGSL) at the lower limit of the subarctic region in eastern Canada is the largest estuarine system in the world, and is characterized by an exceptional richness in environmental diversity. It is among the world's most intensively studied estuaries, yet there are no published data on its surface-water pCO_2 distribution. To fill this data gap, a comprehensive dataset was compiled from direct and indirect measurements of carbonate system parameters in the surface waters of the EGSL during the spring or summer of 2003–2016. The calculated pCO_2 ranged from 435–765 µatm in the shallow, partially mixed Upper Estuary, 139–578 µatm in the deep, stratified Lower Estuary, and 207–478 µatm along the Laurentian Channel in the Gulf. Overall, at the time of sampling, the St. Lawrence Estuary served as a weak source of CO_2 to the atmosphere, with an area-averaged CO_2 degassing flux of 1.00 to 2.06 mmol C m^{-2} d^{-1} (0.37 to 0.75 mol C m^{-2} yr^{-1}). A preliminary analysis of factors controlling the spatial variability of surface-water pCO_2 reveals that respiration (Upper Estuary), photosynthesis (Lower Estuary), and temperature (Gulf) are dominant controls.

Keywords:
Coastal ocean, Estuaries, CO_2, Carbon cycle, Air-sea CO_2 exchange, St. Lawrence Estuary, Gulf of St. Lawrence, Laurentian Channel

1. Introduction

Biogeosciences Discuss., doi:10.5194/bg-2017-1, 2017
Manuscript under review for journal Biogeosciences
Published: 19 January 2017

Although estuaries occupy a very small fraction (0.2 %) of the global ocean surface area, their CO_2 emissions are disproportionately large compared with CO_2 exchanges between the open ocean and the atmosphere (Bauer et al., 2013). With an estimated global efflux of 0.25 ± 0.25 Pg C yr^{-1} (Regnier et al., 2013), estuarine CO_2 degassing is thought to counterbalance CO_2 uptake on the continental shelves (Laruelle et al., 2010; Cai, 2011). Almost every estuary on Earth, for which data are available, is generally supersaturated with CO_2 with respect to the atmosphere (Cai and Wang, 1998; Frankignoulle et al., 1998; Borges, 2005; Borges et al., 2005; Borges et al., 2006; Chen and Borges, 2009; Laruelle et al., 2010; Cai, 2011; Chen et al., 2012; Bauer et al., 2013; Chen et al., 2013; Regnier et al., 2013), with values of partial pressure of CO_2 (pCO_2) ranging from 400 to 10,000 µatm (in contrast, the atmospheric pCO_2 in coastal zones was approximately 360–385 µatm in year 2000) (Cai, 2011). Although estuaries are generally net sources of CO_2, there is considerable variability and uncertainty in estimates of their CO_2 emissions, reflecting the limited spatial and temporal coverage of pCO_2 measurements in estuaries as well as their heterogeneous nature (hydrological and geomorphological differences, differences in magnitude and stoichiometry of carbon and nutrient inputs) (Bauer et al., 2013; Regnier et al., 2013).

Estuaries are geochemical reaction vessels through which continentally weathered organic matter and inorganic nutrients must pass to enter the coastal ocean (Kaul and Froelich, 1984). Horizontal transport is controlled by a set of physical attributes (tides, wind, bathymetry, basin geography, river flow) that determine the estuarine filter function (Cloern, 2001). The longer the freshwater flushing (or turnover) time of the estuary, the more opportunity there is for water-column biological activity, benthic exchanges and particle-dissolved phase interactions to influence its biogeochemistry (Statham, 2012). The high pCO_2 observed in estuaries results from the *in situ* microbial degradation of internally and externally supplied organic carbon and the lateral transport of inorganic carbon from rivers, coastal wetlands and ground waters (Bauer et al., 2013). In strongly tidal (macrotidal) systems, long water and particle residence times (on the order of weeks to months; Middelburg and Herman, 2007) allow for the extensive modification and degradation of particulate organic carbon during estuarine transport (Borges et al., 2006; Chen and Borges, 2009). In the absence of seasonal or permanent water stratification, the decoupling between production and degradation of organic matter at and below the surface, respectively,

Biogeosciences Discuss., doi:10.5194/bg-2017-1, 2017
Manuscript under review for journal Biogeosciences
Published: 19 January 2017

71 does not occur, resulting in less efficient export of dissolved inorganic carbon (Borges,
72 2005). Strongly tidal estuaries also tend to exhibit lower levels of photosynthetic activity
73 (Monbet, 1992) and have greater suspended particulate matter concentrations within
74 their high-turbidity regions (Uncles et al., 2002; Middelburg and Herman, 2007) where
75 suspended particles and organic-rich aggregates serve as "hot spots" of microbial
76 recycling (Statham, 2012). Field measurements suggest that 10 % of the CO_2 emissions
77 from the inner estuary of macrotidal systems is sustained by the ventilation of riverine
78 CO_2, whereas 90 % is due to local net heterotrophy (Borges et al., 2006) fueled by
79 inputs of terrestrial and riverine-algae derived (planktonic) detritus and, in populated
80 areas, sewage (Chen and Borges, 2009).
81
82 North American estuaries rank first in terms of global estuarine surface area (41
83 %) but account for the lowest numerically averaged CO_2 flux per unit area (12 %)
84 among all continents (Chen et al., 2013). These estimates are subject to large
85 uncertainties due to data paucity. A recent synthesis by Regnier et al. (2013) highlights
86 the meagre spatial coverage of estuarine pCO_2 measurements, particularly along the
87 Canadian eastern seaboard. Ironically, the Estuary and Gulf of St. Lawrence (EGSL) in
88 eastern Canada is the largest semi-enclosed estuarine system in the world, and is
89 among the world's most intensively studied estuaries (El-Sabh and Silverberg, 1990),
90 but was left unmentioned in recent global (Cai, 2011; Chen et al., 2012; Chen et al.,
91 2013) and regional (Laruelle et al., 2015) data compilations. Furthermore, the majority
92 of previous estuarine CO_2 studies have focused on small-scale river-dominated
93 estuaries, whereas there has been limited research on CO_2 dynamics in large estuaries
94 and bay systems (Joesoef et al., 2015) including the areas of mixing at sea (outer
95 estuaries or river plumes) (Borges et al., 2005). A comparative study by Jiang et al.
96 (2008) reveals large differences in CO_2 degassing between marine-dominated and
97 river-dominated estuaries while several authors note that outer estuaries (plumes) can
98 differ substantially from inner (inland) estuaries in terms of CO_2 emissions
99 (Frankignoulle et al., 1998; Borges, 2005; Chen et al., 2012). On the U.S. east coast, the
100 ratio of non-riverine (flushed by tidal action and receiving minimum freshwater inputs)
101 to river-dominated estuaries is nearly 1:1, demonstrating the geographic importance
102 of coastal estuaries/bays on the eastern seaboard of North America (Cai, 2011).
103

Biogeosciences Discuss., doi:10.5194/bg-2017-1, 2017
Manuscript under review for journal Biogeosciences
Published: 19 January 2017

104 The large-scale (width often considerably greater than the internal Rossby
105 radius; Cyr et al., 2015), macrotidal (mean tidal range greater than 2–4 m; Monbet,
106 1992) St. Lawrence Estuary is an excellent analogue of marine-dominated systems.
107 Throughout its length, the full spectrum of oceanic variability can be found (Mertz and
108 Gratton, 1990). Moreover, the basin characteristics and water transport time scales of
109 the St. Lawrence Estuary provide an almost ideal natural laboratory for geochemical
110 studies. Its surface waters have a renewal time of several months while its bottom
111 waters take several years to replenish, allowing for the comparison of spatial-temporal
112 variations in physical and chemical properties (El-Sabh and Silverberg, 1990). Given its
113 bimodal bathymetry, the St. Lawrence Estuary also permits the investigation of
114 biogeochemical processes in two types of estuary: (1) the shallow, partially mixed
115 Upper Estuary where physical mixing and abiotic processes dominate, and (2) the
116 deep, stratified Lower Estuary where biological cycling and oceanic processes prevail
117 (Yeats, 1990). As yet, no systematic study of the surface-water pCO_2 distribution in the
118 St. Lawrence has been published and, hence, the present study provides the first
119 comprehensive description of its mixed-layer inorganic carbon chemistry, including (1)
120 a multi-year compilation of springtime and summertime pCO_2 calculated from field
121 measurements of alkalinity and pH; (2) an area-averaged estimate of the air-sea CO_2
122 gas flux; and (3) an analysis of the relative importance of thermodynamic (temperature)
123 and biological (photosynthesis, respiration) processes in controlling the spatial
124 variability of estuarine pCO_2.
125
126 **2. Materials and methods**
127
128 **2.1. Study area—St. Lawrence Estuary and Gulf**
129
130 The greater St. Lawrence system (Fig. 1) connects the chain of Great Lakes, the
131 second largest terrestrial freshwater reservoir in the world, to the Atlantic Ocean (Yang
132 et al., 1996). With a drainage basin of approximately 1.32 million km^2, the St. Lawrence
133 River channels the second largest freshwater discharge (11,900 $m^3 s^{-1}$) on the North
134 American continent, second only to that of the Mississippi (El-Sabh and Silverberg,
135 1990). The catchment area geology is dominated by silicate rocks of the Precambrian
136 Shield and carbonates of the Paleozoic lowlands, whose components influence the
137 downstream evolution of river chemistry (Yang et al., 1996). The erosion of the

Biogeosciences Discuss., doi:10.5194/bg-2017-1, 2017
Manuscript under review for journal Biogeosciences
Published: 19 January 2017

carbonate rocks of the drainage basin is practically constant, as the quantity of bicarbonate ions carried by the river varies little from season to season (Pelletier and Lebel, 1979). On a yearly basis, between 15–20 % of the outflow of dissolved inorganic carbon from the St. Lawrence River into its estuary originates from the system's tributaries (e.g., Ottawa River, Mascouche River) while 80–85 % is from the Great Lakes (Hélie et al., 2002). The St. Lawrence Estuary (SLE) begins at the landward limit of the salt water intrusion near Île d'Orléans (5 km downstream of Québec City) and stretches 400 km seaward to Pointe-des-Monts where it widens into the Gulf of St. Lawrence (GSL) (El-Sabh and Silverberg, 1990), a semi-enclosed sea with an area of approximately 240,000 km^2 (Dufour and Ouellet, 2007) connected to the Atlantic Ocean through Cabot Strait and the Strait of Belle Isle (Coote and Yeats, 1979).

Traditionally, the SLE is divided into two segments based on its bathymetry and hydrographical features (Ingram and El-Sabh, 1990). The Upper St. Lawrence Estuary (USLE), from Île d'Orléans, just downstream of Québec City, to Tadoussac, near the mouth of the Saguenay Fjord, covers an area of 3,470 km^2. It is relatively narrow (2 to 24 km wide) and mostly shallow (depths less than 30 m; d'Anglejan, 1990), and features an uneven, fairly complex bottom topography characterized by several disconnected channels and troughs separated by ridges and islands (El-Sabh and Murty, 1990). Topographically modified motions give rise to very large tidal ranges and currents (up to 10 m and 3 m s^{-1}, respectively; Mertz and Gratton, 1990). In this tidally energetic region, wind mixing is one to two orders of magnitude smaller than tidal mixing (Painchaud et al., 1995). Owing to the resuspension of bottom sediments (tide, wind or wave generated) and the net non-tidal estuarine circulation (d'Anglejan and Smith, 1973), a well-developed turbidity maximum stretches between Île d'Orléans and Île-aux-Coudres (Painchaud and Therriault, 1989) where suspended particulate matter concentrations vary from 10 to more than 200 mg l^{-1} (Silverberg and Sundby, 1979). The sources of particulate organic matter (POM) in the estuary are still debated (Gearing and Pocklington, 1990). Carbon isotope studies indicate that less than half of the POM is derived from terrestrial sources (Pocklington and Leonard, 1979) and is quite refractory to biodegradation (Lucotte et al., 1991), whereas the major contributor to POM is believed to be "fresh" organic matter, i.e., living or recently living material, of river-borne origin (Tan and Strain, 1983; Hélie and Hillaire-Marcel, 2006). During the spring freshet in April–May, when freshwater discharge delivers 40 % of the annual

Biogeosciences Discuss., doi:10.5194/bg-2017-1, 2017
Manuscript under review for journal Biogeosciences
Published: 19 January 2017

172 solid inputs to the estuary, the input of terrigenous POM is equivalent to the average
173 POM kept in suspension in the turbidity maximum (Lucotte, 1989).
174
175 The Lower St. Lawrence Estuary (LSLE) is fairly unique in that its character is more
176 oceanic than most estuaries due to its grand size in all three dimensions and
177 unimpeded connection with Labrador and Slope waters from the Atlantic Ocean (El-
178 Sabh and Silverberg, 1990). Relative to the USLE, the LSLE is much larger (9,350 km^2;
179 d'Anglejan, 1990), wider (30 to 50 km) and deeper (~300 m), and displays a smoother,
180 less variable bottom topography. Tidal currents are weaker (on the order of 30 cm s^{-1}
181 or less; Mertz and Gratton, 1990) and, under these less turbulent conditions, the Lower
182 Estuary is the major sink of continental inputs to the St. Lawrence system. Most (~75 %)
183 of the terrigenous POM carried by the St. Lawrence River is deposited on the LSLE floor
184 (Lucotte et al., 1991). The dominant bathymetric feature is the Laurentian Channel (or
185 Trough), a deep, central, U-shaped glaciated valley that extends 1,240 km from the
186 eastern Canadian continental shelf break through the GSL and into the LSLE
187 (d'Anglejan, 1990). The termination (head) of the Laurentian Channel at an abrupt and
188 shallow sill near Tadoussac, at the mouth of the Saguenay Fjord, marks the region of
189 transition between the Upper and Lower Estuary and is an area of complex tidal
190 phenomena (Gratton et al., 1988). Due to rapid shoaling, tidal movements, including
191 internal tides and strong flows over the steep sill, locally generate significant mixing of
192 near-surface waters with deeper saline waters, resulting in an important feeding habitat
193 for several large marine mammals (Dufour and Ouellet, 2007) as well as a nutrient-rich
194 surface layer that flows continuously through the LSLE (Coote and Yeats, 1979; Saucier
195 and Chassé, 2000). The Lower Estuary's seaward outflow, together with the Gaspé
196 Current, a rapidly moving coastal jet, are a major input of nutrients and zooplankton to
197 the near-surface waters of the GSL (Coote and Yeats, 1979; Plourde and Runge, 1993).
198 Mesoscale features such as coastal jets, internal Kelvin waves, baroclinic eddies and
199 unstable waves are all possible due to strong Coriolis effects (Ingram and El-Sabh,
200 1990).
201
202 The Lower St. Lawrence Estuary is one of the most laterally stratified estuaries in
203 the world (Larouche et al., 1987). During summertime, the SLE can be described as a
204 three-layer system on the basis of thermal stratification (Gratton et al., 1988). Each
205 spring, a new surface layer flow is initiated by the freshwater runoff from the St.

Biogeosciences Discuss., doi:10.5194/bg-2017-1, 2017
Manuscript under review for journal Biogeosciences
Published: 19 January 2017

Lawrence River, Saguenay Fjord and rivers on the north shore of the estuary (Dufour and Ouellet, 2007; see Fig. 1). Discharge from the St. Lawrence River (mean annual discharge of 10,000 m^3 s^{-1}, peaking at 15,000 m^3 s^{-1} during the spring freshet; Painchaud and Therriault, 1989) provides about 80 % of the total freshwater input to the estuary (Ingram and El-Sabh, 1990), whereas the combined runoff from the Saguenay and Manicouagan rivers accounts for most of the remainder (Tee, 1990). The warm and relatively fresh surface layer (0 to 30 m) overlies the cold intermediate layer or CIL (30–150 m deep; S_P = 32.0 to 32.6) that is formed by the advection of the wintertime surface mixed layer from the GSL (Galbraith, 2006). Below the CIL, a warmer (2 to 6 °C) and saltier (S_P = 33 to 35) bottom layer (>150 m deep), originating from the mixing of western-central Atlantic and Labrador shelf waters that intrude at depth primarily through Cabot Strait, flows sluggishly landward (~0.5 cm s^{-1}; Bugden, 1988) toward the head region of the Laurentian Channel (Saucier et al., 2003; Gilbert et al., 2005).

2.2. Water-column sampling and analytical procedures

Water samples were collected on board the RV *Coriolis II* during ten research cruises within the St. Lawrence Estuary and Gulf in the spring or summer season between 2003 and 2016. The sampling locations are shown in Fig. 2. Samples were taken at ~3m depth and throughout the water column, along the central axis of the estuary and Laurentian Channel, and in the freshwaters of the St. Lawrence River near Québec City, to obtain freshwater and seawater end-member values. A comprehensive dataset describing the inorganic carbon chemistry in surface mixed layer waters was compiled from field measurements of temperature (T), practical salinity (S_P), pH_{NBS} and/or pH_T, total alkalinity (TAlk), soluble reactive phosphate (SRP), and dissolved silicate (DSi), nitrate (NO_3) and oxygen (DO).

T and S_P were determined *in situ* using the conductivity-temperature-depth (CTD) probe (SeaBird SBE 911) mounted on the sampling rosette. The temperature probe was calibrated by the manufacturer, whereas the conductivity sensor was calibrated by the manufacturer and recalibrated using discrete salinity samples collected throughout the water column and analyzed on a Guildline Autosal 8400 salinometer calibrated with IAPSO standard seawater. Water samples destined for pH

Biogeosciences Discuss., doi:10.5194/bg-2017-1, 2017
Manuscript under review for journal Biogeosciences
Published: 19 January 2017

and TAlk measurements were transferred directly from the 12L Niskin bottles mounted on the CTD-rosette system to, respectively, 125mL plastic bottles without headspace and 250mL glass bottles as soon as the rosette was secured onboard. In the latter case, a few crystals of $HgCl_2$ were added before the bottle was sealed with a ground-glass stopper and Apiezon® Type-M high-vacuum grease.

pH was determined onboard at 25 °C, potentiometrically on the NBS/NIST scale (infinite dilution convention, pH_{NBS}) for low salinity waters (S_P < 5) and potentiometrically and/or colorimetrically on the total hydrogen ion concentration scale (constant ionic medium convention, pH_T) for higher salinity waters. Potentiometric pH measurements were carried out using a Radiometer Analytical® GK2401C combination glass electrode connected to a Radiometer Analytical® PHM84 pH/millivolt-meter. Prior to each measurement, the electrode was calibrated against three NIST-traceable buffer solutions: pH-4.00, pH-7.00 and pH-10.00 at 25°C. The electrode response to these buffers was then least-squares fitted to obtain the Nernstian slope. For S_P > 5, pH measurements were converted to the pH_T scale using TRIS buffer solutions prepared at S_P = 5, 15, 25, or 35 for which the pH_T was assigned at 25°C (Millero, 1986). Colorimetric pH measurements were carried out using a Hewlett-Packard UV-Visible diode array spectrophotometer (HP-8453A) and a 5cm quartz cell after thermal equilibration of the sampling bottles in a constant temperature bath at 25.0 ± 0.1°C. Phenol red (Robert-Baldo et al., 1985) and *m*-cresol purple (Clayton and Byrne, 1993) were used as color indicators. The pH_T of the water samples and buffer solutions were calculated according to the equation of Byrne (1987). The reproducibility of the pH measurements was typically better than ± 0.003.

TAlk was measured at McGill University using an automated Radiometer (TitraLab865®) potentiometric titrator and a Red Rod® combination pH electrode (pHC2001). The dilute HCl titrant was calibrated prior, during, and after each titration session using certified reference materials provided by Andrew Dickson (Scripps Institute of Oceanography). Raw titration data were processed with a proprietary algorithm specifically designed for shallow end-point detection. The reproducibility of the method was better than 0.5 %.

Biogeosciences Discuss., doi:10.5194/bg-2017-1, 2017
Manuscript under review for journal Biogeosciences
Published: 19 January 2017

DO concentrations were determined by Winkler titration (Grasshoff et al., 1999) on distinct water samples recovered directly from the Niskin bottles. The relative standard deviation, based on replicate analyses of samples recovered from the same Niskin bottle, was better than 1 %. These measurements further served to calibrate the SBE-43 oxygen probe mounted on the rosette. For the determination of nutrient concentrations, aliquots of the water samples taken from the Niskin bottles were syringe filtered through a 0.45µm Millipore polycarbonate (MA) filter. DSi was measured onboard on the same day of sampling using the method described in Grasshoff et al. (1999). Water samples destined for NO_3 and SRP measurements were transferred, respectively, into acid-washed 15ml polyethylene and borosilicate tubes, quickly frozen and stored at –20 °C. Their concentrations were determined using standard colorimetric methods adapted from Grasshoff et al. (1999) with a SEAL Autoanalyzer III at the Institut des Sciences de la Mer de Rimouski. The analytical detection limit was 0.04 µM for NO_3, 0.05 µM for SRP and 0.1 µM for DSi. Based on replicate analyses of the standards, the reproducibility of these measurements was typically 1 %.

The *in situ* pressure and density of the samples were calculated from the Thermodynamic Equation of Seawater – 2010 (TEOS-10) using the Gibbs Seawater (GSW) Oceanographic Toolbox (MATLAB-version 3.05; McDougall and Barker, 2011). All field measurements reported in µmol L^{-1} were converted to µmol kg^{-1} using the *in situ* density data.

2.3. Calculation of aqueous pCO_2

2.3.1. pCO_2 in surface mixed layer waters

Aqueous pCO_2 ($pCO_{2(water)}$) is defined as the partial pressure of carbon dioxide in wet (100 % water-saturated) air that is in equilibrium with the water sample. Values of $pCO_{2(water)}$ (µatm) and total dissolved inorganic carbon, or DIC (µmol kg^{-1}), were calculated from the measured pH (total or NBS scale) and TAlk (µmol kg^{-1}), at *in situ* temperature (°C), salinity (S_P) and pressure (dbar), using the program CO2SYS (MATLAB-version 1.1; van Heuven et al., 2011) and the carbonic acid dissociation constants, K_1 and K_2, of Cai and Wang (1998) for estuarine waters. Wherever data were

Biogeosciences Discuss., doi:10.5194/bg-2017-1, 2017
Manuscript under review for journal Biogeosciences
Published: 19 January 2017

available, the contributions to TAlk from phosphate and silicate were included. Although the K_1 and K_2 formulations from Lueker et al. (2000) are recommended for best practices by Dickson et al. (2007), they are not suitable for the low-salinity conditions found in estuaries (S_P < 19) (Orr et al., 2015). The revised equations for K_1 and K_2 from Cai and Wang (1998) are applicable over a larger range of salinities (0 to 40) and, thus, were used to examine the carbonate system in the estuarine waters of our study area.

This study focuses on the inorganic carbon dynamics of near-surface waters. To obtain individual data points of surface-water pCO_2 at each sampling location, the $pCO_{2(water)}$ data in the surface mixed layer (SML) were averaged. The SML is the site of active air-sea interaction where heat and gases are exchanged directly with the atmosphere and within which physical (temperature, salinity, density) and chemical (dissolved gases) properties are vertically homogeneous due to turbulent mixing (Sprintall and Tomczak, 1992). The lower limit to air-sea interaction, i.e., the mixed layer depth (MLD), is demarcated by the pycnocline, a sharp density gradient that generally coincides with both a temperature (thermocline) and salinity (halocline) gradient. Here, we determine the thickness of the SML using a density-based criterion, in which the MLD is defined as the depth at which a threshold difference of 0.03 kg m^{-3} from the sea surface occurs (de Boyer Montégut et al., 2004). In the following sections, surface-water pCO_2 will be taken to mean the SML-averaged pCO_2.

2.3.2. Sources of error in pCO_2 calculation

The importance of using appropriate formulations of K_1 and K_2 in estuarine waters is shown by the discrepancies in calculated values of pCO_2 (pH/TAlk) at low salinities (Fig. 3). The percent difference between pCO_2 values calculated from the dissociation constants of Cai and Wang (1998) and those from Lueker et al. (2000) was on average 2.12 %. Calculations differed by 1.13–18.5 % at low salinities (S_P < 19), whereas, at S_P > 19, the calculated pCO_2 were much closer (only ~1.49 % difference). The K_1 and K_2 formulations of Millero (2010), i.e., the most recent alternative proposed for estuarine waters (S_P = 1 to 50), yielded pCO_2 values that differed substantially from those of Cai and Wang (1998) at S_P < 19, with the largest divergence reaching 34.5 % (average difference of 13.7 %). At S_P = 0, the pCO_2 values calculated from Cai and

Biogeosciences Discuss., doi:10.5194/bg-2017-1, 2017
Manuscript under review for journal Biogeosciences
Published: 19 January 2017

Wang (1998) compared very well with those given by the Millero (1979) constants for freshwater (difference of only ~0.08 %), whereas the pCO_2 values calculated from Millero (2010) showed very poor agreement with the freshwater results (differing by ~34.3 %). These discrepancies highlight the need for new or revised measurements of the carbonic acid dissociation constants under estuarine conditions (in brackish waters) especially at $S_P < 5$. Studies which use the best-practices formulations of K_1 and K_2 to calculate estuarine pCO_2 may underestimate CO_2 emissions at low salinities, whereas those that implement the Millero (2010) formulations may produce overestimates.

Another potential source of error in the calculation of pCO_2 (pH/TAlk) in low-salinity estuarine waters is the contribution of organic species to the total alkalinity. While the contributions of borate, phosphate and silicate species are taken into consideration by the program CO2SYS, the magnitude of organic alkalinity (Org-Alk) is usually assumed to be small or negligible, and is simply ignored when using TAlk to calculate pCO_2 in open ocean waters. In riverine and coastal waters, however, the contribution of organic species to the TAlk can be significant (Yang et al., 2015). Rivers draining organic-rich soils and non-carbonate rocks have low DIC concentrations (a few hundred μmol L^{-1}) that are often exceeded by dissolved organic carbon (DOC) concentrations (Abril et al., 2015). As discussed by Hunt et al. (2011), a significant contribution of Org-Alk (the organic acid anions in DOC) leads to an overestimation of calculated pCO_2 using any program that accounts only for the inorganic species contributing to TAlk. A comparison of the calculated TAlk (DIC/pH) (direct DIC measurements were carried out in 2014) and the measured TAlk reveals that Org-Alk is on the order of –20 μmol kg^{-1} for the St. Lawrence River end-member, whereas it is as high as –120 μmol kg^{-1} for the Saguenay River end-member (A. Mucci, pers. comm.). Given that TAlk exceeds ~1000 μmol kg^{-1} throughout our study area and the Saguenay River contribution to the surface waters of the SLE is limited (at most ~6 % at the head of the estuary; Mucci et al., submitted), consideration of the Org-Alk in the calculation of pCO_2 (pH/TAlk) yielded values that were at most 1.9 % different from those uncorrected for Org-Alk. Bearing in mind the uncertainties in the K_1 and K_2 formulations as well as the measurement uncertainties, the influence of Org-Alk on the calculation of pCO_2 (pH/TAlk) did not represent a significant source of error.

2.4. Temperature normalization of pCO_2

Biogeosciences Discuss., doi:10.5194/bg-2017-1, 2017
Manuscript under review for journal Biogeosciences
Published: 19 January 2017

375

376 The effect of temperature on aqueous pCO_2 is primarily the manifestation of
377 changes in the solubility of CO_2 gas in water (Takahashi et al., 1993). The temperature
378 dependence of pCO_2 in seawater, i.e., $\partial \ln(pCO_2) / \partial T = 0.0423\ °C^{-1}$, was determined
379 experimentally by Takahashi et al. (1993) on a single North Atlantic surface water
380 sample with $S_P = 35.380$ under isochemical conditions. As this oft-used approximation
381 for thermally induced changes in pCO_2 was derived from direct measurements in
382 seawater, we use a different approach to remove the temperature effect on the
383 estuarine pCO_2 in our study area. The *in situ* pCO_2 were normalized to the average
384 surface-water temperature (SST = 7.82 °C) using the temperature normalization
385 method of Jiang et al. (2008) in which pCO_2 are re-calculated from the TAlk and DIC
386 data at a common temperature. The results yielded a temperature coefficient of ∂
387 $\ln(pCO_2) / \partial T = 0.0404\ °C^{-1}$ ($R^2 = 0.99$), in excellent agreement with that of Takahashi et
388 al. (1993). The pCO_2 changes due to temperature deviations from the mean SST were
389 calculated as:

390

391 $$\Delta pCO_{2(thermal)} = pCO_{2(in-situ)} - pCO_{2(temp-norm)} \quad (1)$$

392

393 where $\Delta pCO_{2(thermal)}$ is the pCO_2 change due to temperature effects, $pCO_{2(in\text{-}situ)}$ is the
394 *in situ* pCO_2 and $pCO_{2(temp\text{-}norm)}$ is the temperature-normalized pCO_2. Since changes in
395 pCO_2 at a constant temperature primarily reflect changes in DIC, the spatial variations
396 in temperature-normalized pCO_2 were attributed to the combined influences of non-
397 thermal processes, i.e., water mass mixing and biological activity. Theoretically,
398 $pCO_{2(temp\text{-}norm)}$ can be further partitioned into the pCO_2 change due to biology and
399 pCO_2 due to mixing through an analysis of the water mass structure, e.g., an optimum
400 multiparameter (OMP) water mass analysis. Results from its application will be
401 presented in a subsequent study.

402

403 **2.5. Air-sea CO_2 flux estimation**

404

405 Air-sea CO_2 gas exchange (F, mmol C m^{-2} d^{-1}) at each sampling location was
406 estimated as follows:

407

408 $$F = k \cdot K_0 \cdot \left(pCO_{2(water)} - pCO_{2(air)}\right) \quad (2)$$

Biogeosciences Discuss., doi:10.5194/bg-2017-1, 2017
Manuscript under review for journal Biogeosciences
Published: 19 January 2017

where k (cm h^{-1}) is the gas transfer velocity of CO_2, K_0 (mol kg^{-1} atm^{-1}) is the solubility coefficient of CO_2 at *in situ* surface-water temperature and salinity (Weiss, 1974), and $pCO_{2(water)}$ and $pCO_{2(air)}$ (µatm) are the partial pressures of CO_2 in the water and the air, respectively. The difference between $pCO_{2(water)}$ and $pCO_{2(air)}$ (ΔpCO_2) determines the direction of gas exchange across the air-sea interface. Positive values of F indicate release of CO_2 by the surface water, whereas negative values indicate CO_2 uptake by the surface water. Conversion factors were applied to express the final F with the aforementioned units.

Atmospheric pCO_2 ($pCO_{2(air)}$) was calculated using the monthly averages of the measured mole fraction of CO_2 in dry air (xCO_2, at the greenhouse gas observational station in Fraserdale, Ontario) obtained from the Climate Research Division at Environment and Climate Change Canada. The mean $pCO_{2(air)}$ in the sampling month was computed using the relationship (Takahashi et al., 2002):

$$pCO_{2(air)} = xCO_2 \cdot (P_b - P_w) \quad (3)$$

where xCO_2 is in ppm, P_b (atm) is the atmospheric (or barometric) pressure at the sea surface, and P_w (atm) is the equilibrium (or saturation) water vapor pressure at *in situ* surface-water temperature and salinity (Weiss and Price, 1980). One-month averaged barometric pressures were calculated using the hourly station pressure data from Environment Canada at the following weather observing stations: Québec/Jean Lesage International Airport (Upper Estuary), Mont-Joli Airport (Lower Estuary), and Gaspé Airport (Gulf of St. Lawrence). The P_b at station elevation was converted to mean sea level pressure using the formula of Tim Brice and Todd Hall (NOAA's National Weather Service, http://www.weather.gov/epz/wxcalc_stationpressure).

The formulation of the gas transfer velocity, k, is the largest source of error in the computation of air-sea CO_2 fluxes (Borges et al., 2004a,b). Properly constraining values of k in estuaries is problematic (Raymond and Cole, 2001) due to their hydrodynamic and geomorphologic complexity (Abril et al., 2000). Gas transfer is thought to be regulated by turbulence at the air-water interface (Wanninkhof, 1992). Wind stress plays a key role in the generation of turbulence at the ocean surface through the

Biogeosciences Discuss., doi:10.5194/bg-2017-1, 2017
Manuscript under review for journal Biogeosciences
Published: 19 January 2017

transfer of momentum to waves and currents (Ho et al., 2011), whereas, in estuarine environments and especially macrotidal estuaries, surface turbulence can be created by interactions of wind forcing, tidal currents and boundary friction (Zappa et al., 2003, Borges et al., 2004a,b; Zappa et al., 2007) and, in turbid estuaries, attenuated by suspended material (Abril et al., 2009). The turbulence generated from bottom stress varies with water depth and tidal velocity (Raymond et al., 2000), and is important only in shallower estuaries with high current speeds (Cerco, 1989). Raymond and Cole (2001) have shown that wind stress controls turbulence at the air-water interface for all systems with depths greater than 10 meters (at depths < 10 m, either wind or bottom stress may dominate).

Several different predictive relationships between wind speed and gas transfer have been proposed based on laboratory and field studies. Here, we estimate the gas transfer velocity from short-term (or steady) wind speed measurements using the equations of Wanninkhof (1992) revised by Wanninkhof (2014) and Raymond and Cole (2001):

k from Wanninkhof (2014), denoted as $k_{W\text{-}14}$:

$$k_{W-14} = 0.251\, u^2 (Sc\ /\ 660)^{-0.5} \quad (4)$$

k from Raymond and Cole (2001), denoted as $k_{R\&C\text{-}01}$:

$$k_{R\&C-01} = 1.91\, e^{0.35u} (Sc\ /\ 660)^{-0.5} \quad (5)$$

where u is the wind speed (m s^{-1}) and Sc is the Schmidt number (Sc = μ/D, where μ is the kinematic viscosity of the water and D is the diffusion coefficient) for CO_2 gas in solution. The Schmidt number for CO_2 in seawater at 20 °C is 660 and was adjusted to Sc=600 for freshwater. Hourly wind speed data were obtained from Environment Canada at the aforementioned weather observing stations, and averaged over the sampling month to obtain short-term wind speeds. The correction to a common Schmidt number was performed using the equations of Wanninkhof (1992) for the temperature dependence of Sc for CO_2 gas in seawater (S_P=35) and freshwater, respectively, and assuming that k is proportional to $Sc^{-0.5}$.

Biogeosciences Discuss., doi:10.5194/bg-2017-1, 2017
Manuscript under review for journal Biogeosciences
Published: 19 January 2017

476 Because of increased turbulence, one would expect k values calculated from
477 estuarine parameterizations to be higher than those predicted from oceanic
478 parameterizations at equivalent wind speeds (Abril et al., 2000). Within the confines of
479 the SLE, estimates of k using the Wanninkhof (2014) relationship ranged from 1.6 to
480 4.5 cm h^{-1} whereas those calculated from Raymond and Cole (2001) were between 3.8
481 and 8.1 cm h^{-1}. Hence, we take the air-sea CO_2 flux values calculated with $k_{W\text{-}14}$ to be
482 the theoretical lower limit of gas exchange ($F_{W\text{-}14}$), whereas those computed from $k_{R\&C\text{-}01}$
483 represent the upper limit of gas exchange ($F_{R\&C\text{-}01}$).
484
485 In order to estimate the area-averaged CO_2 flux in the SLE, the estuary proper
486 was divided into five segments, with each section containing at least one sampling
487 location. The fluxes for each segment were normalized to the sectional surface area
488 and then summed to obtain a spatially integrated CO_2 flux ($F_{area\text{-}avg}$) for air-sea gas
489 exchange in the whole estuary as follows (Jiang et al., 2008):
490
491 $$F_{area-avg} = \frac{\sum F_i \cdot S_i}{\sum S_i} \quad (6)$$
492
493 where F_i is the average of all the fluxes within segment i, and S_i is the surface area of
494 segment i. Sectional surface areas were tabulated in MATLAB using the land mask of
495 eastern Canada obtained from Fisheries and Oceans Canada. An area-averaged CO_2
496 flux was obtained for both the upper and lower limits of gas exchange in the SLE. These
497 two final estimates are assumed to bracket the real areal CO_2 flux.
498
499 **2.6. Conceptual framework for the analysis of variations in biogenic gas**
500 **concentrations**
501
502 A comparison of the distribution of biologically reactive dissolved gases, e.g.,
503 CO_2 and O_2, can provide useful information about the physical (thermal) and biological
504 processes controlling their concentrations (Richey et al., 1988). Temperature-related
505 gas solubility effects occur in the same direction for CO_2 and O_2, whereas biological
506 production and respiration affect CO_2 and O_2 in opposite directions. Following the
507 approach of Carrillo et al. (2004), the saturation states (or % saturation) of pCO_2 and
508 DO, with respect to the atmosphere, were compared in order to determine the relative
509 importance of temperature changes (heating or cooling) and biological activity

Biogeosciences Discuss., doi:10.5194/bg-2017-1, 2017
Manuscript under review for journal Biogeosciences
Published: 19 January 2017

(photosynthesis or respiration) in the surface waters at each sampling location. The pCO_2 percent saturation ($\%pCO_{2(sat)}$) was calculated as follows:

$$\%pCO_{2(sat)} = \left(pCO_{2(water)} \,/\, pCO_{2(air)}\right) \cdot 100 \quad (7)$$

The DO percent saturation ($\%DO_{(sat)}$) was calculated as:

$$\%DO_{(sat)} = (DO/DO^*) \cdot 100 \quad (8)$$

where DO^* is the equilibrium DO concentration (μmol kg^{-1}) at *in situ* surface-water temperature and salinity (Benson and Krause, 1984).

According to the method of Carrillo et al. (2004), data points fall into one of four quadrants on a graph of $\%DO_{(sat)}$ versus $\%pCO_{2(sat)}$, with the origin at 100 % saturation for both gases. Quadrant I (upper left; supersaturated DO, undersaturated pCO_2) suggests net photosynthesis, Quadrant II (upper right; supersaturated DO and pCO_2) indicates the effects of heating, Quadrant III (lower right; undersaturated DO, supersaturated pCO_2) implies net respiration, and Quadrant IV (lower left; undersaturated DO and pCO_2) represents the effects of cooling. Although general patterns become apparent, we urge caution in the interpretation of these results as significant limitations apply. Surface-water CO_2 and O_2 may be acted upon by other forcings such as air-sea gas exchange. The net transfer of CO_2 and O_2 gases occurs across the air-sea interface whenever their partial pressures in the surface water differ from those in the atmosphere. Because of their differential gas exchange rates (i.e., O_2 exchanges ~19 times faster than CO_2; Peng et al., 1987), CO_2 and O_2 dynamics may be decoupled in surface waters, causing an asymmetry in the observed CO_2:O_2 relationship (Carrillo et al., 2004).

3. Results and discussion

3.1. Spatial variability of surface-water pCO_2

Data were compiled from all ten cruises to describe the inorganic carbon chemistry in the SML waters of the St. Lawrence River, Upper Estuary, Lower Estuary

Biogeosciences Discuss., doi:10.5194/bg-2017-1, 2017
Manuscript under review for journal Biogeosciences
Published: 19 January 2017

and Gulf (Table 1). Large spatial variations in surface-water pCO_2 were observed in the EGSL system, with values ranging from 139 to 765 µatm (453 ± 133 µatm) during the spring/summer sampling periods. The pCO_2 were higher in the USLE (571 ± 72 µatm) than in the LSLE (394 ± 117 µatm) and GSL (354 ± 82 µatm), whereas the atmospheric pCO_2 showed less variability, ranging from 372 to 405 µatm, during the sampling months. From Fig. 4, it can be seen that the USLE was always a CO_2 source ($pCO_{2(water)}$ above atmospheric equilibrium) while the LSLE and GSL were generally either a CO_2 sink or nearly neutral ($pCO_{2(water)}$ below or close to atmospheric equilibrium).

Within the confines of the SLE, the surface-water pCO_2 generally decreased with increasing distance from the head of the estuary (Île d'Orléans) and along the salinity gradient (Fig. 4 and 5). The highest values of pCO_2 were observed near the landward limit of the salt water intrusion in the SLE's upper reaches, in the vicinity of the Cap Tourmente intertidal flats and marshes. This area (3×10^6 m^2) is located along the core of the estuary's maximum turbidity zone (MTZ) (Lucotte and d'Anglejan, 1986). The lowest surface-water pCO_2 were found downstream of the MTZ in the lower reaches of the SLE near Pointe-des-Monts, where the channel widens into the gulf. Due to favorable environmental conditions (nutrients, light, stratification), phytoplankton blooms typically occur in late spring or early summer in the LSLE (Zakardjian et al., 2000), with maximal biological production occurring in its downstream portion due to the mixing of cold, nutrient-rich waters, upwelled at the head of the Laurentian Channel, with warmer freshwaters flowing in from the north shore rivers (Savenkoff et al., 1994). Seaward from the estuary-gulf boundary, the pCO_2 gradually increased from 207 to 478 µatm, coinciding with a large increase in surface-water temperature (T = 3.9 to 13.7 °C).

The spatial variability of surface-water pCO_2 due to temperature variations was removed by normalizing the pCO_2 data to a common temperature (T = 7.82 °C). A comparison of the *in situ* and corresponding temperature-normalized pCO_2 shows that spatial changes in water temperature lower or raise the pCO_2 by –170 to 181 µatm. The maximum (minimum) values of $\Delta pCO_{2(thermal)}$, expressed as a percent change, were 38 % (–14 %) in the USLE, 24 % (–31 %) in the LSLE, and 29 % (–17 %) in the GSL. Temperature normalization, however, removed only a small part of the overall spatial variability of surface-water pCO_2 (Fig. 6). Given that the spread of the temperature-

Biogeosciences Discuss., doi:10.5194/bg-2017-1, 2017
Manuscript under review for journal Biogeosciences
Published: 19 January 2017

normalized pCO_2 data remained large (153–668 µatm; 449 ± 133 µatm), most of the spatial heterogeneity in surface-water pCO_2 can be explained by non-thermal processes (water mass mixing and/or biological activity).

3.2. Air-sea CO_2 flux and spatial integration

Large spatial variability of the air-sea CO_2 flux was observed in the EGSL system during the spring/summer sampling periods, with fluxes ranging from –21.9 to 28.4 mmol m^{-2} d^{-1} (Fig. 7). Values of F were always positive in the USLE (2.0 to 28.4 mmol m^{-2} d^{-1}) and either negative or positive in the LSLE (–21.9 to 15.1 mmol m^{-2} d^{-1}) and GSL (–8.4 to 3.6 mmol m^{-2} d^{-1}). As expected, $F_{R\&C\text{-}01}$ (estuarine parameterization of k) were larger than $F_{W\text{-}14}$ (oceanic parameterization of k) due to the inherently greater surface turbulence in estuarine systems. The average difference between fluxes calculated from Wanninkhof (2014) and those from Raymond and Cole (2001) was 71.5 %. Details of the k and F values given by each parameterization of the gas transfer velocity are shown in Table 2. Irrespective of the parameterization, the calculated CO_2 fluxes were more positive in the USLE (9.2 ± 5.3 mmol m^{-2} d^{-1}) than in the LSLE (0.8 ± 7.1 mmol m^{-2} d^{-1}) and GSL (–1.1 ± 3.0 mmol m^{-2} d^{-1}).

To obtain an area-averaged CO_2 flux for the whole estuary, the SLE was divided into five segments, with each segment containing at least one sampling location. The data used to calculate the area-averaged CO_2 flux are listed in Table 3. Overall, the SLE served as a weak source of CO_2 to the atmosphere at the time of sampling, with an area-averaged CO_2 degassing flux of 1.00 to 2.06 mmol C m^{-2} d^{-1} (0.37 to 0.75 mol C m^{-2} yr^{-1}). This efflux compares favorably with that of the Delaware Estuary (2.4 ± 4.8 mol C m^{-2} yr^{-1}; Joesoef et al., 2015), another large estuarine system with a long water residence time, but is significantly lower than estimates in the marine-dominated Sapelo and Doboy Sound estuaries (10.5 to 10.7 mol C m^{-2} yr^{-1}; Jiang et al., 2008). From a compilation of 165 estuaries worldwide, almost all systems, with the exception of those in the Arctic (–1.1 mol C m^{-2} yr^{-1}), serve as sources of CO_2 to the atmosphere (Chen et al., 2013). Chen et al. (2013) concluded that the world's upper estuaries (S_P < 2) are strong sources (39.0 ± 55.7 mol C m^{-2} yr^{-1}), mid estuaries (2 < S_P < 25) are moderate sources (17.5 ± 34.2 mol C m^{-2} yr^{-1}), and lower estuaries (S_P > 25) are weak sources (8.4 ± 14.3 mol C m^{-2} yr^{-1}). Predictably, with its maritime region occupying

Biogeosciences Discuss., doi:10.5194/bg-2017-1, 2017
Manuscript under review for journal Biogeosciences
Published: 19 January 2017

almost three-fourths of the total surface area, the SLE behaves like an outer estuary with only small CO_2 evasion. The lack of temporal coverage of surface-water pCO_2 data, however, prevents us from reliably synthesizing an annual air-sea CO_2 flux.

3.3. Major controlling factors of estuarine pCO_2

The pCO_2 in the surface mixed layer is a function of its temperature (T), salinity (S_P), dissolved inorganic carbon (DIC) and total alkalinity (TAlk), as described by the following relationship (Takahashi et al., 1993):

$$dpCO_2 = (\partial pCO_2/\partial T)dT + (\partial pCO_2/\partial S_P)dS_P + (\partial pCO_2/\partial DIC)dDIC + (\partial pCO_2/\partial TAlk)dTAlk \quad (9)$$

Through changes in T, S_P, DIC and TAlk, variations in surface-water pCO_2 are mainly controlled by dynamic processes (water mass mixing), thermodynamic processes (temperature and salinity changes), air-sea gas exchange and biological processes (photosynthesis, respiration) (Poisson et al., 1993). Among these, the effects of temperature and DIC, i.e., the DIC inputs from internal (biological activity) and external (physical mixing) sources, are generally the most important drivers of estuarine pCO_2 variability. Whereas the variations in pCO_2 due to water mass mixing and those due to *in situ* biological activity will be separated in a future study through a modified OMP water mass analysis, here, we evaluate the relative importance of thermal and biological processes in controlling the spatial distribution of pCO_2 in our study area.

To disentangle the biological and temperature effects on pCO_2 variability, the $\%DO_{(sat)}$ were plotted against the $\%pCO_{2(sat)}$, with the origin at 100 % saturation for both gases. This simple approach uses the four possible combinations of $\%pCO_{2(sat)}/\%DO_{(sat)}$ as integrated measures of thermally and biologically induced changes. From Fig. 8, it can be seen that microbial respiration was the major driver of pCO_2 variability in the USLE, whereas the effects of photosynthesis and temperature predominated in the LSLE and GSL. In the strongly stratified Lower Estuary, the biological drawdown of pCO_2 surpassed the increasing effect of sea surface warming (Fig. 9). Values of surface-water pCO_2 were mostly below atmospheric level despite increases in temperature (T = –0.32 to 12.6 °C). This pattern is consistent with the

Biogeosciences Discuss., doi:10.5194/bg-2017-1, 2017
Manuscript under review for journal Biogeosciences
Published: 19 January 2017

finding that, in spring/summer, the increasing effect of warming on pCO_2 is counteracted by the photosynthetic utilization of CO_2, particularly in a strongly stratified shallow mixed layer (Takahashi et al., 1993). In the Gulf of St. Lawrence, the temperature dependence of pCO_2 exerted a major influence, causing values of surface-water pCO_2 to increase (207 to 478 µatm) concomitantly with temperature (T = 3.9 to 13.7 °C) (Fig. 9).

4. Conclusions

Because of its large physical dimensions and unimpeded connection to the Atlantic Ocean, the St. Lawrence Estuary encompasses both a river-dominated inner estuary, where physical mixing and abiotic processes dominate, and a marine-dominated outer estuary, where biological cycling and oceanic processes prevail. The physical and biogeochemical processes of these contrasting environments are reflected in the spatial distribution of surface-water pCO_2 (139–765 µatm). The shallow, partially mixed Upper Estuary, with a turbidity maximum controlled by tide- and wind-induced turbulence, was, during our sampling period, a source of CO_2 to the atmosphere due to microbial respiration (low biological productivity), whereas the deep, stratified Lower Estuary, with its stable, summertime three-layer vertical structure, was generally a sink of atmospheric CO_2 due to the enhanced biological drawdown of pCO_2 (light availability, nutrient supply, strong stratification).

Overall, the large subarctic St. Lawrence Estuary was a weak source of CO_2 to the atmosphere, with an area-averaged CO_2 degassing flux of 1.00 to 2.06 mmol C m^{-2} d^{-1} (0.37 to 0.75 mol C m^{-2} yr^{-1}). This efflux is somewhat smaller than the numerically averaged CO_2 flux per unit area (2.19 mol C m^{-2} yr^{-1}) reported from North American estuaries by Chen et al. (2013), highlighting their relatively small contribution (~12 %) to global estuarine CO_2 emissions. The pronounced shift in source/sink dynamics in the St. Lawrence Estuary, between its river-dominated (9.2 ± 5.3 mmol m^{-2} d^{-1}) and marine-dominated (0.8 ± 7.1 mmol m^{-2} d^{-1}) regions, is consistent with the conclusions of the comparative study carried out by Jiang et al. (2008) that showed large differences in CO_2 degassing between riverine (inner) and maritime (outer) estuaries. Given the limited research on CO_2 dynamics in large estuaries and bay systems, which cover approximately one-half of the estuarine surface area on the U.S. east coast, as

Biogeosciences Discuss., doi:10.5194/bg-2017-1, 2017
Manuscript under review for journal Biogeosciences
Published: 19 January 2017

well as the large uncertainties in the calculation of pCO_2 (carbonic acid dissociation constants, organic alkalinity contribution), current global-scale estimates of estuarine CO_2 degassing may be overestimated. To better constrain the role of large estuaries/bays in the estuarine carbon cycle, more extensive spatial and temporal coverage of pCO_2 measurements is needed.

Data availability

Data presented in this paper (Figures 4 and 8) are available upon request from one of the authors (alfonso.mucci@mcgill.ca).

Author contribution

A.D. and A.M. conceived the project. A.M. acquired and processed the data prior to 2016. A.D. conducted the data analysis and wrote the first draft of the paper whereas A.M. provided editorial and scientific recommendations.

Competing interests

The authors declare that they have no conflict of interest.

Acknowledgements

We wish to thank the Captains and crews of the RV *Coriolis II* for their unwavering help over the years. We also wish to acknowledge Gilles Desmeules and Michel Rousseau for their dedicated electronic and field sampling support as well as Constance Guignard for her help in cruise preparation and field data acquisition. Most of the data acquisition was carried out opportunistically on research cruises funded by grants to A.M. or Canadian colleagues by the Natural Sciences and Engineering Research Council of Canada (NSERC) whereas the work was funded by a Regroupement Stratégique grant from the Fonds Québécois de Recherche Nature et Technologies (FQRNT) to GEOTOP as well as NSERC Discovery and MEOPAR grants to A.M. A.D. wishes to thank the Department of Earth and Planetary Sciences at McGill for financial support in the form of scholarships and assistantships.

References

Abril, G., Etcheber, H., Borges, A. V., and Frankignoulle, M.: Excess atmospheric carbon dioxide transported by rivers into the Scheldt estuary, Cr. Acad. Sci. II A., 330, 761–768, 2000.

Abril, G., Commarieu, M. V., Sottolichio, A., Bretel, P., and Guerin, F.: Turbidity limits gas exchange in a large macrotidal estuary, Estuar. Coast. Shelf S., 83, 342–348, 2009.

Abril, G. et al.: Technical Note: Large overestimation of pCO_2 calculated from pH and alkalinity in acidic, organic-rich freshwaters, Biogeosciences, 12, 67–78, 2015.

Bauer, J. E., Cai, W. J., Raymond, P. A., Bianchi, T. S., Hopkinson, C. S., and Regnier, P. A.: The changing carbon cycle of the coastal ocean, Nature, 504, 61–70, 2013.

Benson, B. B. and Krause, D.: The concentration and isotopic fractionation of oxygen dissolved in freshwater and seawater in equilibrium with the atmosphere, Limnol. Oceanogr., 29, 620–632, 1984.

Borges, A. V.: Do we have enough pieces of the jigsaw to integrate CO_2 fluxes in the coastal ocean?, Estuaries, 28, 3–27, 2005.

Borges, A. V., Delille, B., Schiettecatte, L. S., Gazeau, F., Abril, G., and Frankignoulle, M.: Gas transfer velocities of CO_2 in three European estuaries (Randers Fjord, Scheldt and Thames), Limnol. Oceanogr., 49, 1630–1641, 2004a.

Borges, A. V., Vanderborght, J. P., Schiettecatte, L. S., Gazeau, F., Ferrón-Smith, S., Delille, B., and Frankignoulle, M.: Variability of the gas transfer velocity of CO_2 in a macrotidal estuary (the Scheldt), Estuaries, 27, 593–603, 2004b.

Borges, A. V., Delille, B., and Frankignoulle, M.: Budgeting sinks and sources of CO_2 in the coastal ocean: Diversity of ecosystems counts, Geophys. Res. Lett., 32, L14601, doi:10.1029/2005GL023053, 2005.

Borges, A. V., Schiettecatte, L. S., Abril, G., Delille, B., and Gazeau, F.: Carbon dioxide in European coastal waters, Estuar. Coast. Shelf S., 70, 375–387, 2006.

Bugden, G. L.: Oceanographic conditions in the deeper waters of the Gulf of St. Lawrence in relation to local and oceanic forcing, NAFO SCR document 88/87, 1988.

Byrne, R. H.: Standardization of standard buffers by visible spectrometry, Anal. Chem., 59, 1479–1481, 1987.

Cai, W. J.: Estuarine and coastal ocean carbon paradox: CO_2 sinks or sites of terrestrial carbon incineration?, Annual Review of Marine Science, 3, 123–145, 2011.

Biogeosciences Discuss., doi:10.5194/bg-2017-1, 2017
Manuscript under review for journal Biogeosciences
Published: 19 January 2017

754
755 Cai, W. J. and Wang, Y.: The chemistry, fluxes, and sources of carbon dioxide in the estuarine
756 waters of the Satilla and Altamaha Rivers, Georgia, Limnol. Oceanogr., 43, 657–668, 1998.
757
758 Carrillo, C. J., Smith, R. C., and Karl, D. M.: Processes regulating oxygen and carbon dioxide in
759 surface waters west of the Antarctic Peninsula, Mar. Chem., 84, 161–179, 2004.
760
761 Cerco, C. F.: Estimating estuarine reaeration rates, J. Environ. Eng.-ASCE, 115, 1066–1070,
762 1989.
763
764 Chen, C. T. A. and Borges, A. V.: Reconciling opposing views on carbon cycling in the coastal
765 ocean: continental shelves as sinks and near-shore ecosystems as sources of atmospheric CO_2,
766 Deep-Sea Res. Pt. II, 56, 578–590, 2009.
767
768 Chen, C. T. A., Huang, T. H., Fu, Y. H., Bai, Y., and He, X.: Strong sources of CO_2 in upper
769 estuaries become sinks of CO_2 in large river plumes, Current Opinion in Environmental
770 Sustainability, 4, 179–185, 2012.
771
772 Chen, C. T. A., Huang, T. H., Chen, Y. C., Bai, Y., He, X., and Kang, Y.: Air–sea exchanges of CO_2
773 in the world's coastal seas, Biogeosciences, 10, 6509–6544, 2013.
774
775 Clayton, T. D. and Byrne, R. H.: Spectrophotometric seawater pH measurements: total
776 hydrogen ion concentration scale calibration of m-cresol purple and at-sea results, Deep-Sea
777 Res. Pt. I, 40, 2115–2129, 1993.
778
779 Cloern, J. E.: Our evolving conceptual model of the coastal eutrophication problem, Mar. Ecol.-
780 Prog. Ser., 210, 223–253, 2001.
781
782 Coote, A. R. and Yeats, P. A.: Distribution of nutrients in the Gulf of St. Lawrence, J. Fish. Res.
783 Board Can., 36, 122–131, 1979.
784
785 Cyr, F., Bourgault, D., Galbraith, P. S., and Gosselin, M.: Turbulent nitrate fluxes in the Lower St.
786 Lawrence Estuary, Canada, J. Geophys. Res.-Oceans, 120, 2308–2330, 2015.
787
788 d'Anglejan, B.: Recent sediments and sediment transport processes in the St. Lawrence
789 Estuary, in: El-Sabh, M. I. and Silverberg, N. (Eds.), Oceanography of a Large-scale Estuarine
790 System, Springer-Verlag, New York, 109–129, 1990.

Biogeosciences Discuss., doi:10.5194/bg-2017-1, 2017
Manuscript under review for journal Biogeosciences
Published: 19 January 2017

d'Anglejan, B. F. and Smith, E. C.: Distribution, transport, and composition of suspended matter in the St. Lawrence estuary, Can. J. Earth Sci., 10, 1380–1396, 1973.

de Boyer Montégut, C., Madec, G., Fischer, A. S., Lazar, A., and Iudicone, D.: Mixed layer depth over the global ocean: An examination of profile data and a profile-based climatology, J. Geophys. Res., 109, C12003, doi:10.1029/2004JC002378, 2004.

Dickson, A. G. and Goyet, C. (Eds.): Handbook of Methods for the Analysis of the Various Parameters of the Carbon Dioxide System in Sea Water (Version 2), U.S. Department of Energy, ORNL/CDIAC-74, 1994.

Dickson, A. G., Sabine, C. L., and Christian, J. R. (Eds.): Guide to Best Practices for Ocean CO_2 Measurements, PICES Special Publication 3, 191 pp., 2007.

Dufour, R. and Ouellet, P.: Estuary and Gulf of St. Lawrence marine ecosystem overview and assessment report, Can. Tech. Rep. Fish. Aquat. Sci., 2744E, 112 pp., 2007.

El-Sabh, M. I. and Murty, T. S.: Mathematical modelling of tides in the St. Lawrence Estuary, in: El-Sabh, M. I. and Silverberg, N. (Eds.), Oceanography of a Large-scale Estuarine System, Springer-Verlag, New York, 10–50, 1990.

El-Sabh, M. I. and Silverberg, N.: The St. Lawrence Estuary: introduction, in: El-Sabh, M. I. and Silverberg, N. (Eds.), Oceanography of a Large-scale Estuarine System, Springer-Verlag, New York, 1–9, 1990.

Frankignoulle, M. et al.: Carbon dioxide emission from European estuaries, Science, 282, 434–436, 1998.

Galbraith, P. S.: Winter water masses in the Gulf of St. Lawrence, J. Geophys. Res., 111, C06022, doi:10.1029/2005JC003159, 2006.

Gearing, J. N. and Pocklington, R.: Organic geochemical studies in the St. Lawrence Estuary, in: El-Sabh, M. I. and Silverberg, N. (Eds.), Oceanography of a Large-scale Estuarine System, Springer-Verlag, New York, 170–201, 1990.

Biogeosciences Discuss., doi:10.5194/bg-2017-1, 2017
Manuscript under review for journal Biogeosciences
Published: 19 January 2017

827 Gilbert, D., Sundby, B., Gobeil, C., Mucci, A., and Tremblay, G. H.: A seventy-two-year record
828 of diminishing deep-water oxygen in the St. Lawrence estuary: The northwest Atlantic
829 connection, Limnol. Oceanogr., 50, 1654–1666, 2005.
830
831 Grasshoff, K., Kremling, K., and Ehrhardt, M. (Eds.): Methods of Seawater Analysis (3rd ed.),
832 Wiley-VCH, Weinheim, Germany, 1999.
833
834 Gratton, Y., Mertz, G., and Gagné, J. A.: Satellite observations of tidal upwelling and mixing in
835 the St. Lawrence Estuary, J. Geophys. Res.-Oceans, 93, 6947–6954, 1988.
836
837 Hélie, J. F. and Hillaire-Marcel, C.: Sources of particulate and dissolved organic carbon in the
838 St Lawrence River: isotopic approach, Hydrol. Process., 20, 1945–1959, 2006.
839
840 Hélie, J. F., Hillaire-Marcel, C., and Rondeau, B.: Seasonal changes in the sources and fluxes of
841 dissolved inorganic carbon through the St. Lawrence River—isotopic and chemical constraint,
842 Chem. Geol., 186, 117–138, 2002.
843
844 Ho, D. T., Wanninkhof, R., Schlosser, P., Ullman, D. S., Hebert, D., and Sullivan, K. F.: Toward a
845 universal relationship between wind speed and gas exchange: Gas transfer velocities
846 measured with 3He/SF_6 during the Southern Ocean Gas Exchange Experiment, J. Geophys.
847 Res., 116, C00F04, doi:10.1029/2010JC006854, 2011.
848
849 Hunt, C. W., Salisbury, J. E., and Vandemark, D.: Contribution of non-carbonate anions to total
850 alkalinity and overestimation of pCO_2 in New England and New Brunswick rivers,
851 Biogeosciences, 8, 3069–3076, 2011.
852
853 Ingram, R. G. and El-Sabh, M. I.: Fronts and mesoscale features in the St. Lawrence Estuary, in:
854 El-Sabh, M. I. and Silverberg, N. (Eds.), Oceanography of a Large-scale Estuarine System,
855 Springer-Verlag, New York, 71–93, 1990.
856
857 Jiang, L. Q., Cai, W. J., and Wang, Y.: A comparative study of carbon dioxide degassing in river-
858 and marine-dominated estuaries, Limnol. Oceanogr., 53, 2603–2615, 2008.
859
860 Joesoef, A., Huang, W. J., Gao, Y., and Cai, W. J.: Air–water fluxes and sources of carbon
861 dioxide in the Delaware Estuary: spatial and seasonal variability, Biogeosciences, 12, 6085–
862 6101, 2015.
863

Kaul, L. W. and Froelich, P. N.: Modeling estuarine nutrient geochemistry in a simple system, Geochim. Cosmochim. Ac., 48, 1417–1433, 1984.

Larouche, P., Koutitonsky, V. G., Chanut, J. P., and El-Sabh, M. I.: Lateral stratification and dynamic balance at the Matane transect in the lower Saint Lawrence estuary, Estuar. Coast. Shelf S., 24, 859–871, 1987.

Laruelle, G. G., Dürr, H. H., Slomp, C. P., and Borges, A. V.: Evaluation of sinks and sources of CO_2 in the global coastal ocean using a spatially-explicit typology of estuaries and continental shelves, Geophys. Res. Lett., 37, L15607, doi:10.1029/2010GL043691, 2010.

Laruelle, G. G., Lauerwald, R., Rotschi, J., Raymond, P. A., Hartmann, J., and Regnier, P.: Seasonal response of air-water CO_2 exchange along the land-ocean aquatic continuum of the northeast North American coast, Biogeosciences, 12, 1447–1458, 2015.

Lucotte, M.: Organic carbon isotope ratios and implications for the maximum turbidity zone of the St Lawrence upper estuary, Estuar. Coast. Shelf S., 29, 293–304, 1989.

Lucotte, M. and d'Anglejan, B.: Seasonal control of the Saint-Lawrence maximum turbidity zone by tidal-flat sedimentation, Estuaries, 9, 84–94, 1986.

Lucotte, M., Hillaire-Marcel, C., and Louchouarn, P.: First-order organic carbon budget in the St Lawrence Lower Estuary from ^{13}C data, Estuar. Coast. Shelf S., 32, 297–312, 1991.

Lueker, T. J., Dickson, A. G., and Keeling, C. D.: Ocean pCO_2 calculated from dissolved inorganic carbon, alkalinity, and equations for K_1 and K_2: validation based on laboratory measurements of CO_2 in gas and seawater at equilibrium, Mar. Chem., 70, 105–119, 2000.

McDougall, T. J. and Barker, P. M.: Getting started with TEOS-10 and the Gibbs Seawater (GSW) Oceanographic Toolbox, SCOR/IAPSO WG127, ISBN 978-0-646-55621-5, 28 pp., 2011.

Mertz, G. and Gratton, Y.: Topographic waves and topographically induced motions in the St. Lawrence Estuary, in: El-Sabh, M. I. and Silverberg, N. (Eds.), Oceanography of a Large-scale Estuarine System, Springer-Verlag, New York, 94–108, 1990.

Middelburg, J. J. and Herman, P. M.: Organic matter processing in tidal estuaries, Mar. Chem., 106, 127–147, 2007.

Biogeosciences Discuss., doi:10.5194/bg-2017-1, 2017
Manuscript under review for journal Biogeosciences
Published: 19 January 2017

Millero, F. J.: The thermodynamics of the carbonate system in seawater, Geochim. Cosmochim. Ac., 43, 1651–1661, 1979.

Millero, F. J.: The pH of estuarine waters, Limnol. Oceanogr., 31, 839–847, 1986.

Millero, F. J.: Carbonate constants for estuarine waters, Mar. Freshwater Res., 61, 139–142, 2010.

Monbet, Y.: Control of phytoplankton biomass in estuaries: a comparative analysis of microtidal and macrotidal estuaries, Estuaries, 15, 563–571, 1992.

Mucci, A., Levasseur, M., Gratton, Y., Martias, C., Scarratt, M., Gilbert, D., Tremblay, J.-É., Ferreya, G., and Lansard, B.: Tidal-induced variations of pH at the head of the Laurentian Channel, Can. J. Fish. Aquat. Sci. (submitted), 2016.

Orr, J. C., Epitalon, J. M., and Gattuso, J. P.: Comparison of ten packages that compute ocean carbonate chemistry, Biogeosciences Discussions, 12, 1483–1510, 2015.

Painchaud, J. and Therriault, J. C.: Relationships between bacteria, phytoplankton and particulate organic carbon in the upper St. Lawrence estuary, Mar. Ecol.-Prog. Ser., 56, 301–311, 1989.

Painchaud, J., Lefaivre, D., Therriault, J. C., and Legendre, L.: Physical processes controlling bacterial distribution and variability in the upper St. Lawrence estuary, Estuaries, 18, 433–444, 1995.

Pelletier, E. and Lebel, J.: Hydrochemistry of dissolved inorganic carbon in the St. Lawrence Estuary (Canada), Estuar. Coast. Mar. Sci., 9, 785–795, 1979.

Peng, T. H., Takahashi, T., Broecker, W. S., and Olafsson, J.: Seasonal variability of carbon dioxide, nutrients and oxygen in the northern North Atlantic surface water: observations and a model, Tellus, 39B, 439–458, 1987.

Plourde, S. and Runge, J. A.: Reproduction of the planktonic copepod Calanus finmarchicus in the Lower St. Lawrence Estuary: relation to the cycle of phytoplankton production and evidence for a Calanus pump, Mar. Ecol.-Prog. Ser., 102, 217–227, 1993.

Pocklington, R. and Leonard, J. D.: Terrigenous organic matter in sediments of the St. Lawrence Estuary and the Saguenay Fjord, J. Fish. Res. Board Can., 36, 1250–1255, 1979.

Poisson, A., Metzl, N., Brunet, C., Schauer, B., Bres, B., Ruiz-Pino, D., and Louanchi, F.: Variability of sources and sinks of CO_2 in the Western Indian and Southern Oceans during the year 1991, J. Geophys. Res.-Oceans, 98, 22759–22778, 1993.

Raymond, P. A. and Cole, J. J.: Gas exchange in rivers and estuaries: Choosing a gas transfer velocity, Estuar. Coast., 24, 312–317, 2001.

Raymond, P. A., Bauer, J. E., and Cole, J. J.: Atmospheric CO_2 evasion, dissolved inorganic carbon production, and net heterotrophy in the York River estuary, Limnol. Oceanogr., 45, 1707–1717, 2000.

Regnier, P. et al.: Anthropogenic perturbation of the carbon fluxes from land to ocean, Nat. Geosci., 6, 597–607, 2013.

Richey, J. E., Devol, A. H., Wofsy, S. C., Victoria, R., and Riberio, M. N.: Biogenic gases and the oxidation and reduction of carbon in Amazon River and floodplain waters, Limnol. Oceanogr., 33, 551–561, 1988.

Robert-Baldo, G. L., Morris, M. J., and Byrne, R. H.: Spectrophotometric determination of seawater pH using phenol red, Anal. Chem., 57, 2564–2567, 1985.

Roy, R. N. et al.: The dissociation constants of carbonic acid in seawater at salinities 5 to 45 and temperatures 0 to 45°C, Mar. Chem., 44, 249–267, 1993.

Saucier, F. J. and Chassé, J.: Tidal circulation and buoyancy effects in the St. Lawrence Estuary, Atmos. Ocean, 38, 505–556, 2000.

Saucier, F. J., Roy, F., Gilbert, D., Pellerin, P., and Ritchie, H.: Modeling the formation and circulation processes of water masses and sea ice in the Gulf of St. Lawrence, Canada. J. Geophys. Res., 108, 3269, doi:10.1029/2000JC000686, 2003.

Savenkoff, C., Comeau, L., Vézina, A. F., and Gratton, Y.: Seasonal variation of the biological activity in the lower St. Lawrence Estuary, Can. Tech. Rep. Fish. Aquat. Sci., 2006, 22 pp., 1994.

Silverberg, N. and Sundby, B.: Observations in the turbidity maximum of the St. Lawrence estuary, Can. J. Earth Sci., 16, 939–950, 1979.

Sprintall, J. and Tomczak, M.: Evidence of the barrier layer in the surface layer of the tropics, J. Geophys. Res.-Oceans, 97, 7305–7316, 1992.

Statham, P. J.: Nutrients in estuaries—an overview and the potential impacts of climate change, Sci. Total Environ., 434, 213–227, 2012.

Takahashi, T., Olafsson, J., Goddard, J. G., Chipman, D. W., and Sutherland, S. C.: Seasonal variation of CO_2 and nutrients in the high-latitude surface oceans: a comparative study, Global Biogeochem. Cy., 7, 843–878, 1993.

Takahashi, T. et al.: Global sea–air CO_2 flux based on climatological surface ocean pCO_2, and seasonal biological and temperature effects, Deep-Sea Res. Pt. II, 49, 1601–1622, 2002.

Tan, F. C. and Strain, P. M.: Sources, sinks and distribution of organic carbon in the St. Lawrence Estuary, Canada, Geochim. Cosmochim. Ac., 47, 125–132, 1983.

Tee, K-T.: Meteorologically and buoyancy induced subtidal salinity and velocity variations in the St. Lawrence Estuary, in: El-Sabh, M. I. and Silverberg, N. (Eds.), Oceanography of a Large-scale Estuarine System, Springer-Verlag, New York, 51–70, 1990.

Uncles, R. J., Stephens, J. A., and Smith, R. E.: The dependence of estuarine turbidity on tidal intrusion length, tidal range and residence time, Cont. Shelf Res., 22, 1835–1856, 2002.

van Heuven, S., Pierrot, D., Rae, J. W. B., Lewis, E., and Wallace, D. W. R.: MATLAB program developed for CO_2 system calculations, ORNL/CDIAC-105b, Carbon Dioxide Information Analysis Center, Oak Ridge National Laboratory, U.S. Department of Energy, Oak Ridge, Tennessee, doi: 10.3334/CDIAC/otg.CO2SYS_MATLAB_v1.1, 2011.

Wanninkhof, R.: Relationship between wind speed and gas exchange over the ocean, J. Geophys. Res.-Oceans, 97, 7373–7382, 1992.

Wanninkhof, R.: Relationship between wind speed and gas exchange over the ocean revisited, Limnol. Oceanogr.–Meth., 12, 351–362, 2014.

Weiss, R.: Carbon dioxide in water and seawater: the solubility of a non-ideal gas, Mar. Chem., 2, 203–215, 1974.

Weiss, R. F. and Price, B. A.: Nitrous oxide solubility in water and seawater, Mar. Chem., 8, 347–359, 1980.

Working Group on the State of the St. Lawrence Monitoring, Overview of the State of the St. Lawrence 2014, St. Lawrence Action Plan, Environment Canada, Québec's ministère du Développement durable, de l'Environnement et de la Lutte contre les changements climatiques), Québec's ministère des Forêts, de la Faune et des Parcs, Parks Canada, Fisheries and Oceans Canada, and Stratégies Saint-Laurent, 52 pp., 2014.

Yang, B., Byrne, R. H., and Lindemuth, M.: Contributions of organic alkalinity to total alkalinity in coastal waters: A spectrophotometric approach, Mar. Chem., 176, 199–207, 2015.

Yang, C., Telmer, K., and Veizer, J.: Chemical dynamics of the "St. Lawrence" riverine system: δD_{H2O}, $\delta^{18}O_{H2O}$, $\delta^{13}C_{DIC}$, $\delta^{34}S_{sulfate}$, and dissolved $^{87}Sr/^{86}Sr$, Geochim. Cosmochim. Ac., 60, 851–866, 1996.

Yeats, P. A.: Reactivity and transport of nutrients and metals in the St. Lawrence Estuary, in: El-Sabh, M. I. and Silverberg, N. (Eds.), Oceanography of a Large-scale Estuarine System, Springer-Verlag, New York, 155–169, 1990.

Zakardjian, B. A., Gratton, Y., and Vézina, A. F.: Late spring phytoplankton bloom in the Lower St. Lawrence Estuary: the flushing hypothesis revisited, Mar. Ecol.-Prog. Ser., 192, 31–48, 2000.

Zappa, C. J., Raymond, P. A., Terray, E. A., and McGillis, W. R.: Variation in surface turbulence and the gas transfer velocity over a tidal cycle in a macro-tidal estuary, Estuaries, 26, 1401–1415, 2003.

Zappa, C. J., McGillis, W. R., Raymond, P. A., Edson, J. B., Hintsa, E. J., Zemmelink, H. J., Dacey, J. W. H., and Ho, D. T.: Environmental turbulent mixing controls on air-water gas exchange in marine and aquatic systems, Geophys. Res. Lett., 34, L10601, doi:10.1029/2006GL028790, 2007.

Biogeosciences Discuss., doi:10.5194/bg-2017-1, 2017
Manuscript under review for journal Biogeosciences
Published: 19 January 2017

1049 **Table 1.** Mean, standard deviation and range of the surface-water temperature (T),
1050 practical salinity (S_P), dissolved inorganic carbon (DIC), total alkalinity (TAlk) and *in situ*
1051 partial pressure of CO_2 (pCO_2) in the St. Lawrence River (near Québec City), Upper
1052 Estuary (Île d'Orléans to Tadoussac), Lower Estuary (Tadoussac to Pointe-des-Monts)
1053 and Gulf (Pointe-des-Monts to Cabot Strait) during all sampling months.

	T (°C)	S_P	DIC (μmol kg^{-1})	TAlk (μmol kg^{-1})	pCO_2 (μatm)
River (N=3)	14.2 ± 3.9 (9.8–17.2)	0.03 ± 0.05 (0–0.09)	1242 ± 132 (1148–1335)	1204 ± 99 (1124–1314)	604 ± 76 (550–658)
Upper (N=46)	9.6 ± 3.6 (4.2–17.4)	10.9 ± 8.0 (0–24.5)	1514 ± 242 (1081–2005)	1492 ± 272 (969–2030)	571 ± 72 (435–765)
Lower (N=60)	5.6 ± 2.8 (-0.32–12.6)	26.8 ± 2.7 (21.2–32.7)	1843 ± 89 (1634–2083)	1962 ± 87 (1752–2185)	394 ± 117 (139–578)
Gulf (N=30)	8.8 ± 3.1 (3.9–13.7)	30.1 ± 1.5 (25.5–31.5)	1936 ± 64 (1761–2032)	2094 ± 61 (1921–2175)	354 ± 82 (207–478)

Biogeosciences Discuss., doi:10.5194/bg-2017-1, 2017
Manuscript under review for journal Biogeosciences
Published: 19 January 2017

1073 **Table 2.** Mean, standard deviation and range of ΔpCO_2, $k_{W\text{-}14}$, $k_{R\&C\text{-}01}$, $F_{W\text{-}14}$ and $F_{R\&C\text{-}01}$
1074 in the surface waters of the St. Lawrence River, Upper Estuary, Lower Estuary and Gulf
1075 during all sampling months. $k_{W\text{-}14}$ are the gas transfer velocities given by the
1076 Wanninkhof (2014) relationship, whereas $k_{R\&C\text{-}01}$ are those given by Raymond and Cole
1077 (2001). Values of $F_{W\text{-}14}$ are taken to be the theoretical lower limit of air-sea gas
1078 exchange, whereas values of $F_{R\&C\text{-}01}$ are the upper limit; the extreme F data points are
1079 shown in bold.

	ΔpCO_2 (µatm)	$k_{W\text{-}14}$ (cm h^{-1})	$k_{R\&C\text{-}01}$ (cm h^{-1})	$F_{W\text{-}14}$ (mmol m^{-2} d^{-1})	$F_{R\&C\text{-}01}$ (mmol m^{-2} d^{-1})
River (N=3)	217 ± 99 (147–287)	3.0 ± 1.4 (1.9–4.5)	6.1 ± 2.0 (4.3–8.2)	5.8 ± 3.2 (**3.5**–8.0)	12.7 ± 6.4 (8.2–**17.3**)
Upper (N=46)	184 ± 72 (43–386)	2.8 ± 0.8 (1.6–4.5)	5.6 ± 1.1 (3.8–8.1)	6.1 ± 3.0 (**2.0**–14.7)	12.3 ± 5.4 (3.6–**28.4**)
Lower (N=60)	8.7 ± 115 (–266–188)	3.2 ± 0.5 (2.0–3.8)	5.9 ± 0.6 (4.3–6.9)	0.6 ± 4.8 (–12.1–8.3)	1.0 ± 8.9 (**–21.9**–**15.1**)
Gulf (N=30)	–28.4 ± 91 (–178–107)	1.2 ± 0.3 (0.8–1.7)	3.4 ± 0.3 (2.8–4.1)	–0.7 ± 1.5 (–3.6–1.1)	–1.6 ± 3.9 (**–8.4**–**3.6**)

1080
1081
1082
1083
1084
1085
1086
1087
1088
1089
1090
1091
1092
1093
1094
1095

Biogeosciences Discuss., doi:10.5194/bg-2017-1, 2017
Manuscript under review for journal Biogeosciences
Published: 19 January 2017

1096 **Table 3.** Sectional and area-averaged air-sea CO_2 fluxes (mmol C m^{-2} d^{-1}) in the St.
1097 Lawrence Estuary during all sampling months. To obtain the area-averaged CO_2 flux,
1098 the SLE was divided into five segments at equal intervals. The first row of the table
1099 shows the surface area (km^2) of each segment. The flux data in each segment were
1100 numerically averaged to obtain sectional fluxes, which were then area weighted and
1101 summed to obtain the spatially integrated whole-estuary flux (in bold). The $F_{W\text{-}14}$ and
1102 $F_{R\&C\text{-}01}$ data provide the lower and upper estimates, respectively.

	Seg 1 (N=17)	Seg 2 (N=23)	Seg 3 (N=21)	Seg 4 (N=17)	Seg 5 (N=8)	Whole estuary
Surface area (km^2)	1,098	2,250	2,726	3,404	3,303	12,781
$F_{W\text{-}14}$ (mmol m^{-2} d^{-1})	7.2	5.4	4.3	-1.7	-4.0	**1.00**
$F_{R\&C\text{-}01}$ (mmol m^{-2} d^{-1})	14.5	11.0	7.9	-3.3	-7.4	**2.06**

1103
1104
1105
1106
1107
1108
1109
1110
1111
1112
1113
1114
1115
1116
1117
1118
1119
1120
1121
1122
1123
1124
1125

Biogeosciences Discuss., doi:10.5194/bg-2017-1, 2017
Manuscript under review for journal Biogeosciences
Published: 19 January 2017

Figure 1. Map of the greater St. Lawrence system, including the chain of Great Lakes, the St. Lawrence River, the Upper St. Lawrence Estuary (USLE), the Lower St. Lawrence Estuary (LSLE), and the Gulf of St. Lawrence (GSL). From: Overview of the State of the St. Lawrence 2014 (with permission).

Biogeosciences Discuss., doi:10.5194/bg-2017-1, 2017
Manuscript under review for journal Biogeosciences
Published: 19 January 2017

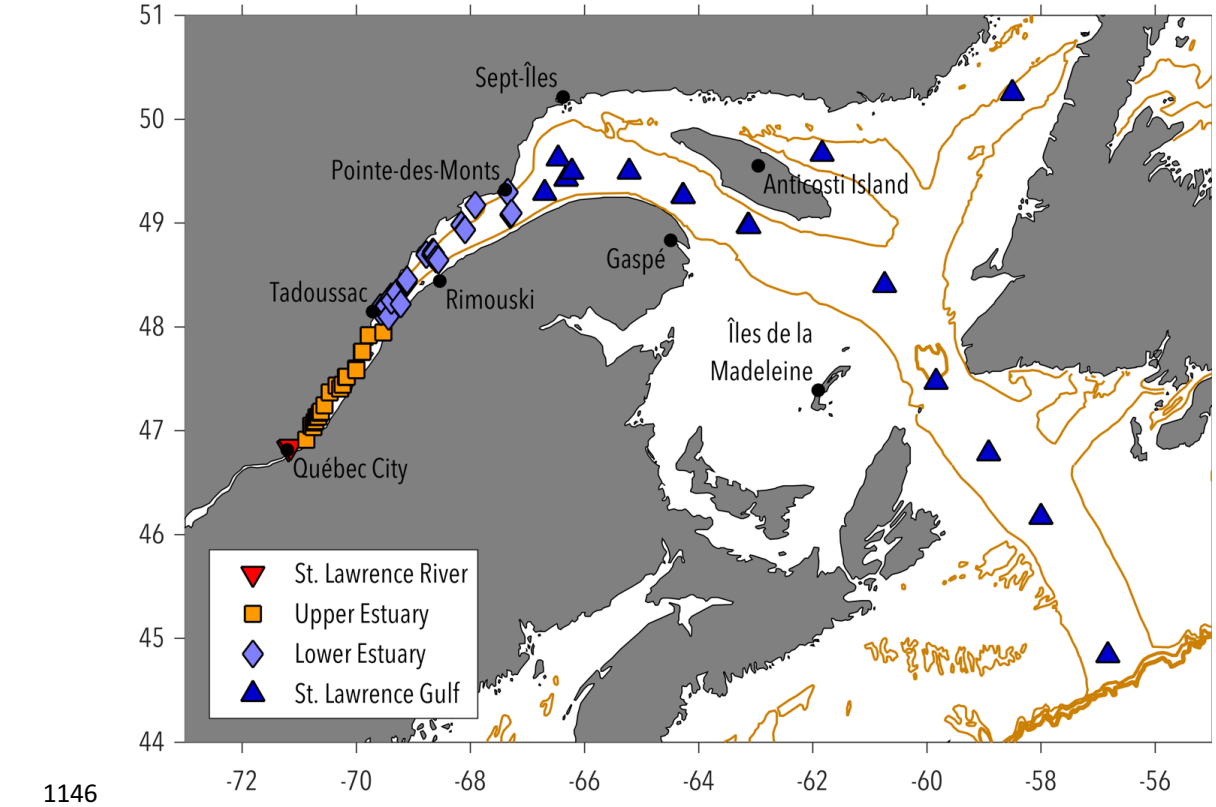

Figure 2. Map showing the four principal subdivisions of the study area and the sampling locations (markers). Water samples were collected during ten spring/summer research cruises: July 2003, June 2006, May 2007, July 2007, June 2009, July 2009, July 2010, May 2011, June 2013 and May 2016. The estuary, from the landward limit of the salt water intrusion near Île d'Orléans (5 km downstream of Québec City) to Pointe-des-Monts, where the coastline diverges, extends ~400 km and covers a total surface area of ~12,820 km^2. The solid gold line follows the 200m isobath of the Laurentian Channel.

Biogeosciences Discuss., doi:10.5194/bg-2017-1, 2017
Manuscript under review for journal Biogeosciences
Published: 19 January 2017

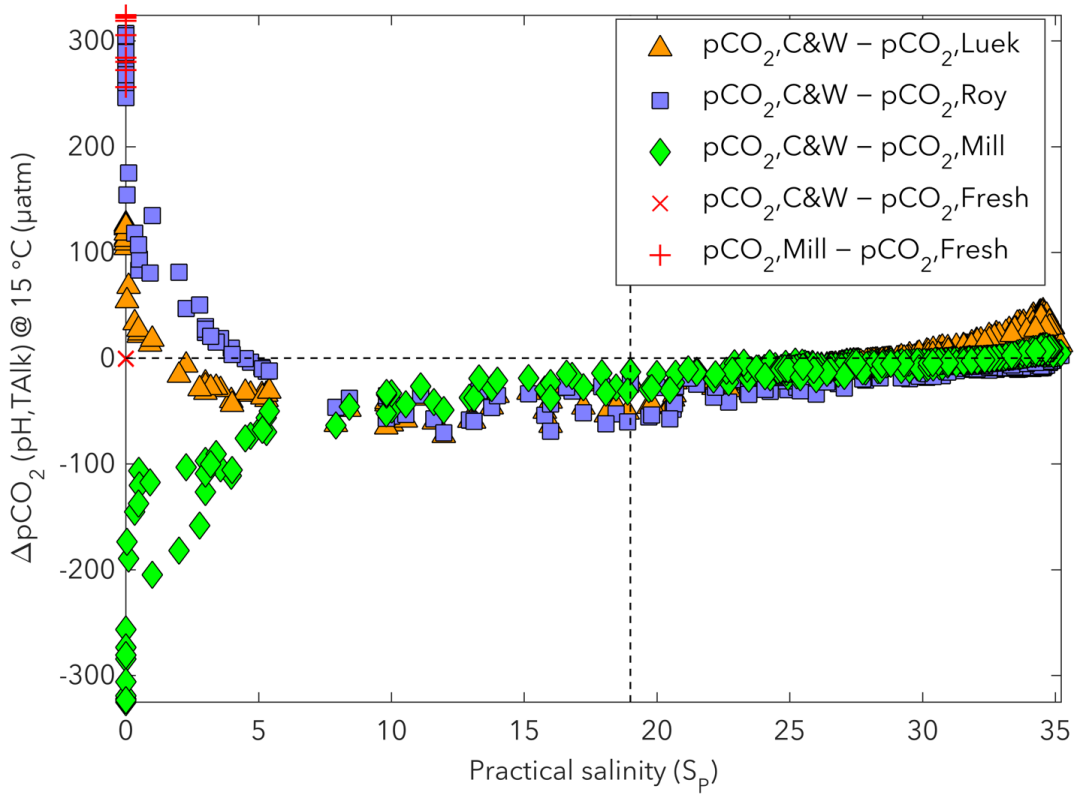

Figure 3. Differences of pCO_2 (ΔpCO_2) calculated from measured pH and TAlk with different published formulations of K_1 and K_2 including Cai and Wang (1998) [C&W], Lueker et al. (2000) [Luek], Roy et al. (1993) [Roy], Millero (2010) [Mill], and Millero (1979) for pure water only (S_P = 0) [Fresh]. All calculations were carried out at 15 °C (pCO_2 @ 15 °C). The constants of Lueker et al. (2000) are recommended for best practices by Dickson et al. (2007), whereas those of Roy et al. (1993) (S_P = 5 to 45) are recommended by Dickson and Goyet (1994). Both the constants of Cai and Wang (1998) and Millero (2010) have been proposed as more appropriate for the study of the carbonate system in estuarine waters.

Biogeosciences Discuss., doi:10.5194/bg-2017-1, 2017
Manuscript under review for journal Biogeosciences
Published: 19 January 2017

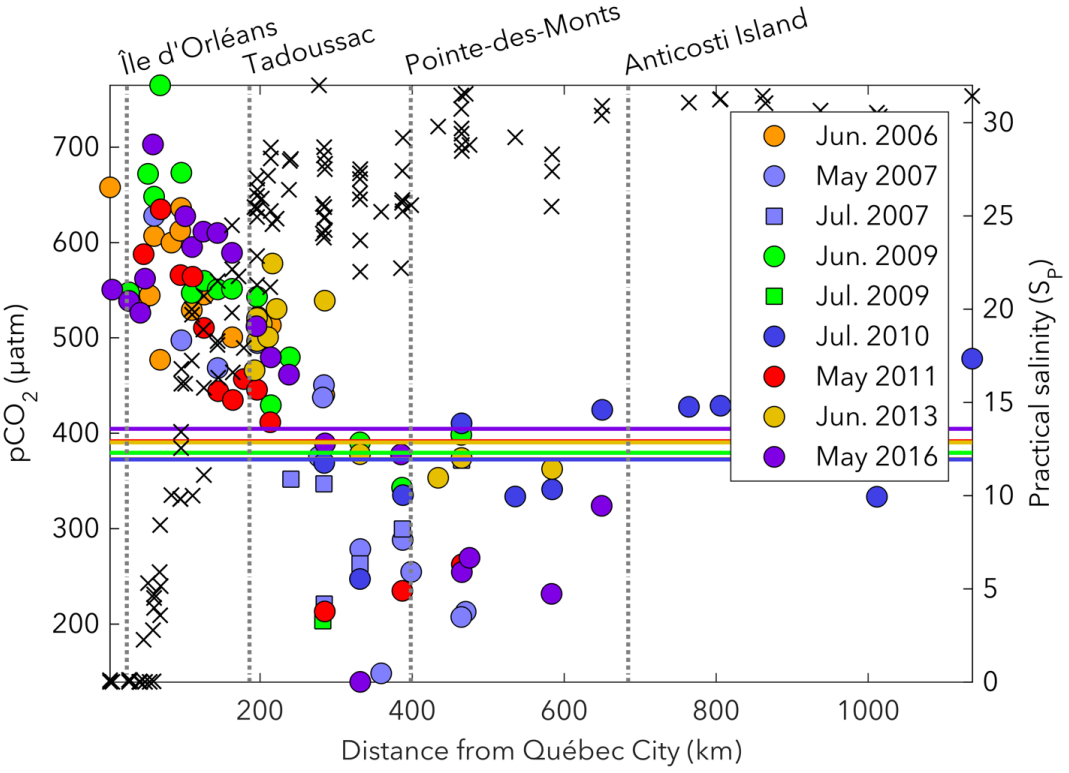

Figure 4. Spatial distributions of surface-water pCO_2 (circles, squares) and practical salinity (x symbols) in the St. Lawrence River, Estuary and Gulf during spring/summer cruises. Horizontal lines show the mean $pCO_{2(air)}$ in the sampling months. The pCO_2 data points above atmospheric level are sources of CO_2 to the atmosphere whereas those below atmospheric level are sinks of atmospheric CO_2.

Biogeosciences Discuss., doi:10.5194/bg-2017-1, 2017
Manuscript under review for journal Biogeosciences
Published: 19 January 2017

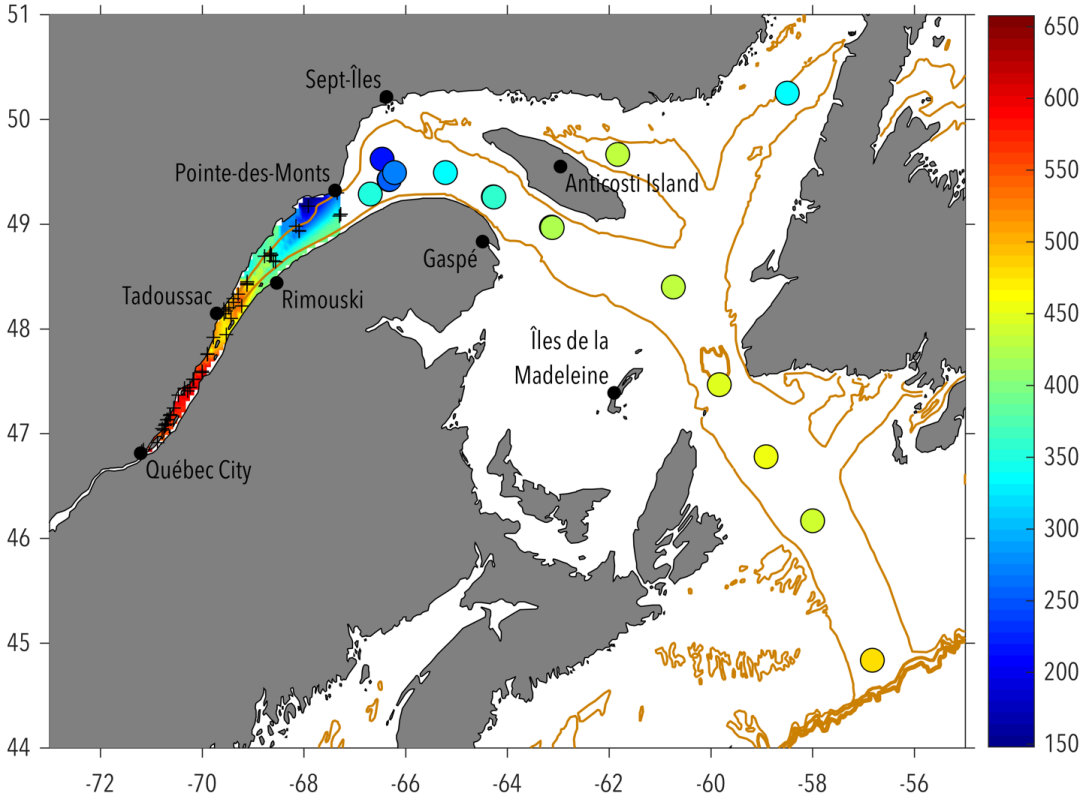

Figure 5. Spatial distribution of surface-water pCO_2 (µatm) in the St. Lawrence Estuary and Gulf during all spring/summer cruises. Linear interpolation was used between the sampling locations (+ symbols). The mean atmospheric pCO_2 during the sampling months ranged from 372 to 405 µatm.

Biogeosciences Discuss., doi:10.5194/bg-2017-1, 2017
Manuscript under review for journal Biogeosciences
Published: 19 January 2017

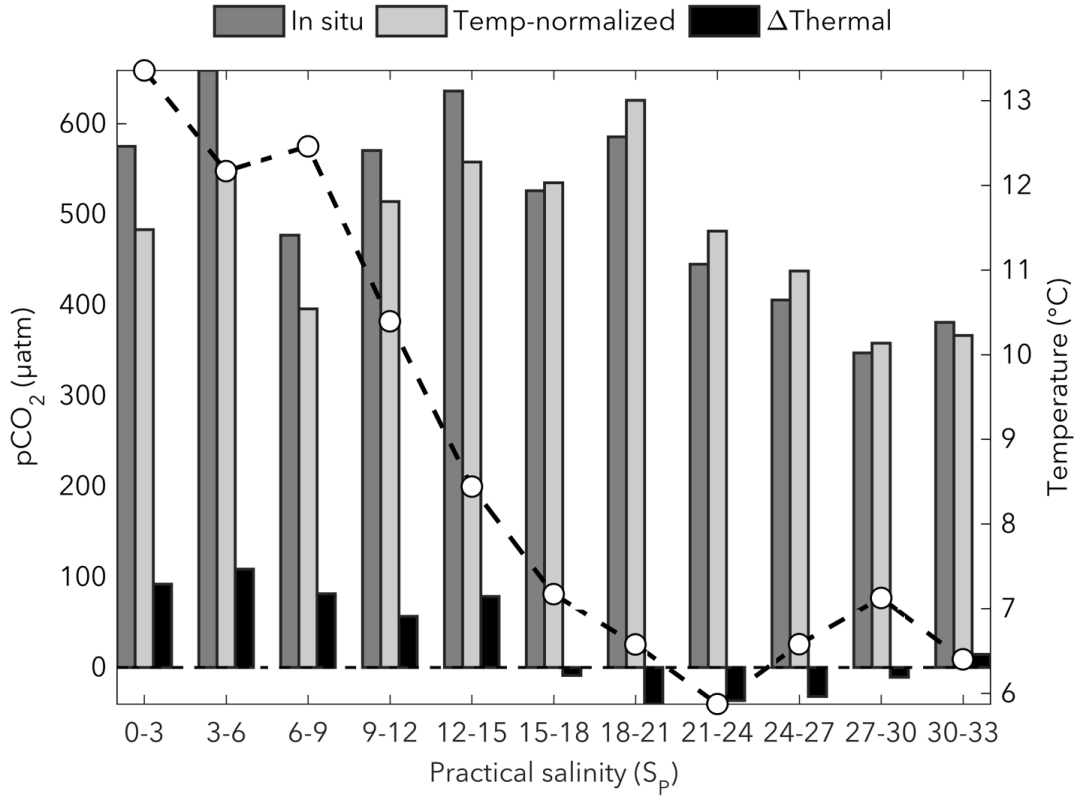

Figure 6. The surface-water *in situ* pCO_2, temperature-normalized pCO_2, and $\Delta pCO_{2(thermal)}$ averaged over salinity bins of 3. The open circles show the average temperature for each salinity bin. To correct for the increasing/decreasing effect of temperature on surface-water pCO_2, the *in situ* pCO_2 were normalized to the average surface-water temperature of the study area (T = 7.82 °C). The $\Delta pCO_{2(thermal)}$ are due to temperature deviations from T = 7.82 °C, whereas variations in temperature-normalized pCO_2 are due to water mass mixing and/or biological activity.

Biogeosciences Discuss., doi:10.5194/bg-2017-1, 2017
Manuscript under review for journal Biogeosciences
Published: 19 January 2017

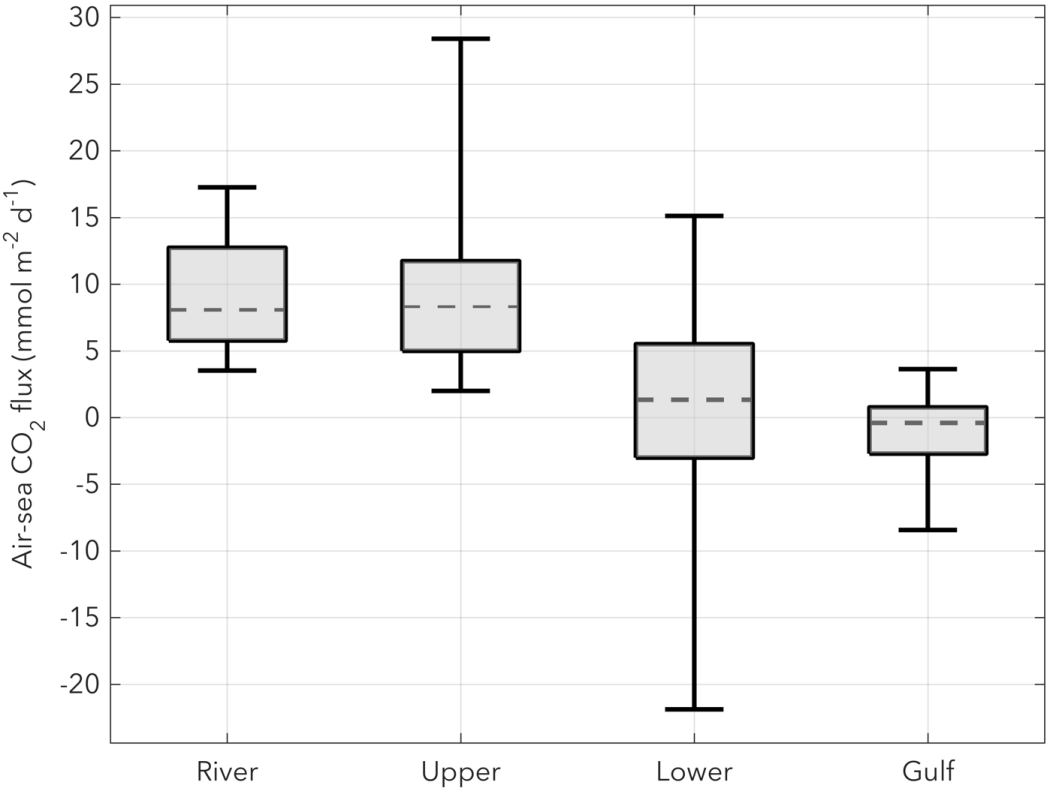

Figure 7. Box plot showing the variability of air-sea CO_2 fluxes in the four principal subdivisions of the study area (St. Lawrence River, Upper Estuary, Lower Estuary and Gulf). The box spans the interquartile range (25–75 percentiles), the dashed line is the median, and the whiskers extend to the extreme data points. The $F_{W\text{-}14}$ data were combined with the $F_{R\&C\text{-}01}$ data from all spring/summer sampling months to depict the upper and lower limits of gas exchange.

Biogeosciences Discuss., doi:10.5194/bg-2017-1, 2017
Manuscript under review for journal Biogeosciences
Published: 19 January 2017

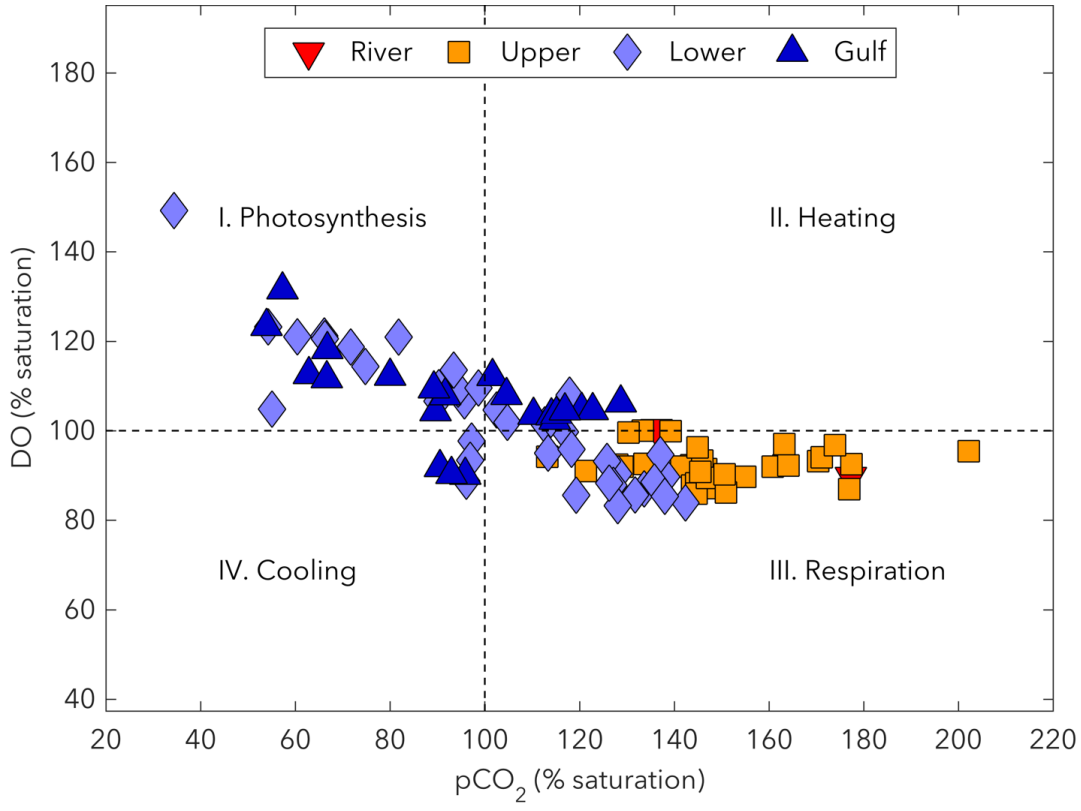

Figure 8. Comparison of the saturation states (or % saturation) of pCO_2 and DO in the surface mixed layer waters of the St. Lawrence River, Estuary and Gulf. Dashed lines delineate the 100 % saturation levels for both gases. Surface-water samples (markers) fall into one of four quadrants representing the dominant controls on CO_2/O_2 dynamics. Quadrants I and III indicate the effects of photosynthesis/respiration, whereas Quadrants II and IV indicate the effects of heating/cooling.

Biogeosciences Discuss., doi:10.5194/bg-2017-1, 2017
Manuscript under review for journal Biogeosciences
Published: 19 January 2017

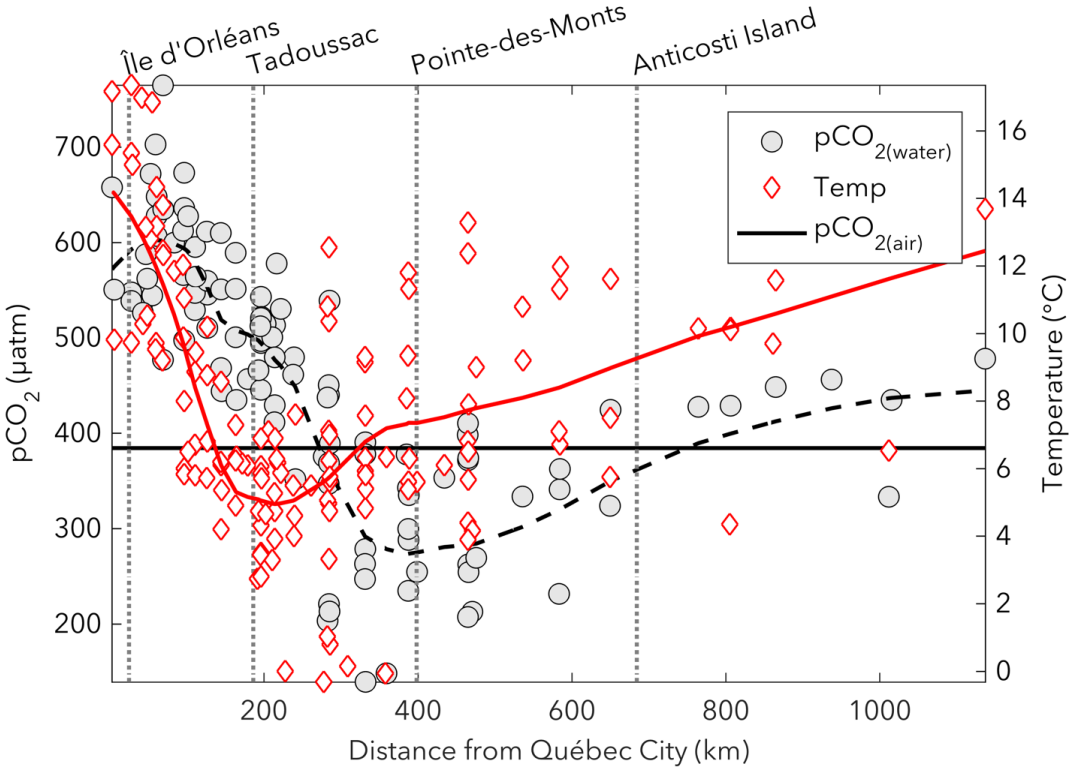

Figure 9. Spatial distributions of surface-water pCO_2 (circles) and temperature (diamonds) in the St. Lawrence River, Estuary and Gulf during spring/summer cruises. Temperatures ranged from 4.2 to 17.4 °C (generally decreasing) in the USLE, –0.32 to 12.6 °C (generally increasing) in the LSLE, and 3.9 to 13.7 °C (generally increasing) in the GSL. The horizontal line shows the mean atmospheric pCO_2, $pCO_{2(air)}$, during all sampling months.